NAVAL POSTGRADUATE SCHOOL

MONTEREY, CALIFORNIA

THESIS

RECEIVE CHANNEL ARCHITECTURE AND TRANSMISSION SYSTEM FOR DIGITAL ARRAY RADAR

by

Yoke Chuang Yong

December 2005

Thesis Advisor:	David Jenn
Co-Advisor:	Donald Walters

Approved for public release, distribution is unlimited

THIS PAGE INTENTIONALLY LEFT BLANK

REPORT DOCUMENTATION PAGE			Form Approved OMB No. 0704-0188
Public reporting burden for this collection of information is estimated to average 1 hour per response, including the time for reviewing instruction, searching existing data sources, gathering and maintaining the data needed, and completing and reviewing the collection of information. Send comments regarding this burden estimate or any other aspect of this collection of information, including suggestions for reducing this burden, to Washington headquarters Services, Directorate for Information Operations and Reports, 1215 Jefferson Davis Highway, Suite 1204, Arlington, VA 22202-4302, and to the Office of Management and Budget, Paperwork Reduction Project (0704-0188) Washington DC 20503.			
1. AGENCY USE ONLY *(Leave blank)*	**2. REPORT DATE** December 2005	**3. REPORT TYPE AND DATES COVERED** Master's Thesis	
4. TITLE AND SUBTITLE: Receive Channel Architecture and Transmission System for Digital Array Radar			**5. FUNDING NUMBERS**
6. AUTHOR(S) Yoke Chuang Yong			
7. PERFORMING ORGANIZATION NAME(S) AND ADDRESS(ES) Naval Postgraduate School Monterey, CA 93943-5000			**8. PERFORMING ORGANIZATION REPORT NUMBER**
9. SPONSORING /MONITORING AGENCY NAME(S) AND ADDRESS(ES) N/A			**10. SPONSORING/MONITORING AGENCY REPORT NUMBER**
11. SUPPLEMENTARY NOTES The views expressed in this thesis are those of the author and do not reflect the official policy or position of the Department of Defense or the U.S. Government.			
12a. DISTRIBUTION / AVAILABILITY STATEMENT Approved for public release; distribution is unlimited			**12b. DISTRIBUTION CODE**

13. ABSTRACT (maximum 200 words)

An "opportunistic array" is a new digital antenna concept where phased array elements are placed at available open areas over the entire length of the platform. The elements are self-standing transmit-receive modules that require no hardwire connections other than prime power. All synchronization signals and data are passed wirelessly between the elements and a central signal processor. An opportunistic array that is integrated into the hull or superstructure of the warship is called an "aperstructure".

This research investigates a wireless local oscillator distribution in the laboratory, which is a necessary requirement for the coherent operation of the array elements. The research also investigates the digitization and synchronization of multiple receive modules with the local oscillator that will determine the viability of the opportunistic array.

The wireless distribution of data and control signals between the digital beamformer and transmit/receive modules requires a low-loss, wideband, simple to implement transmission system that is integrated into the structure of the warship. This research investigates several transmission structures and compare their performances.

14. SUBJECT TERMS Phased Array, Opportunistic Phased Array, Aperstructure, Radar, Transmitter, Receiver, Quadrature Demodulation, COTS, Wireless Distribution, Transmission System			**15. NUMBER OF PAGES** 94
			16. PRICE CODE
17. SECURITY CLASSIFICATION OF REPORT Unclassified	**18. SECURITY CLASSIFICATION OF THIS PAGE** Unclassified	**19. SECURITY CLASSIFICATION OF ABSTRACT** Unclassified	**20. LIMITATION OF ABSTRACT** UL

NSN 7540-01-280-5500 Standard Form 298 (Rev. 2-89)
Prescribed by ANSI Std. 239-18

THIS PAGE INTENTIONALLY LEFT BLANK

Approved for public release, distribution is unlimited

RECEIVE CHANNEL ARCHITECTURE AND TRANSMISSION SYSTEM FOR DIGITAL ARRAY RADAR

Yoke Chuang Yong
Lieutenant Colonel, Republic of Singapore Air Force
B.Eng., University of London, 1992

Submitted in partial fulfillment of the
requirements for the degree of

MASTER OF SCIENCE IN COMBAT SYSTEMS TECHNOLOGY

from the

NAVAL POSTGRADUATE SCHOOL
December 2005

Author: Yong, Yoke Chuang

Approved by: Professor David C. Jenn
Thesis Advisor

Professor Donald L. Walters
Co-Advisor

James H. Luscombe
Chairman, Department of Physics

THIS PAGE INTENTIONALLY LEFT BLANK

ABSTRACT

An “opportunistic array” is a new digital antenna concept where phased array elements are placed at available open areas over the entire length of the platform. The elements are self-standing transmit-receive modules that require no hardwire connections other than prime power. All synchronization signals and data are passed wirelessly between the elements and a central signal processor. An opportunistic array that is integrated into the hull or superstructure of the warship is called an “aperstructure”.

This research investigates a wireless local oscillator distribution in the laboratory, which is a necessary requirement for the coherent operation of the array elements. The research also investigates the digitization and synchronization of multiple receive modules with the local oscillator that will determine the viability of the opportunistic array.

The wireless distribution of data and control signals between the digital beamformer and transmit/receive modules requires a low-loss, wideband, simple to implement transmission system that is integrated into the structure of the warship. This research investigates several transmission structures and compares their performances.

THIS PAGE INTENTIONALLY LEFT BLANK

TABLE OF CONTENTS

I. INTRODUCTION....1
A. MOTIVATION....1
B. PREVIOUS WORK....3
C. SCOPE OF RESEARCH....4
D. ORGANIZATION OF THESIS....5

II. PHASED ARRAY RADAR AND DIGITAL ANTENNA ARCHITECTURE....7
A. LINEAR PHASED ARRAY....7
1. Array Factor and Radiation Pattern....8
2. Bandwidth Limitations....10
3. Mutual Coupling between Elements....11
B. MULTI-DIMENSIONAL AND CONFORMAL ARRAY CONCEPT....12
C. THINNED ARRAY – APERIODIC AND RANDOM....12
D. OPPORTUNISTIC ARRAY CONCEPT....13
E. DIGITAL ANTENNA ARCHITECTURE....15
F. WIRELESS LO DISTRIBUTION FOR DIGITAL ANTENNA CONCEPT....17
G. QUADRATURE DEMODULATION SCHEME....18
H. FREQUENCY SELECTION....19
I. SUMMARY....20

III. PHASE CHARACTERISTICS OF QUADRATURE DEMODULATOR....21
A. ANALOG DEVICES AD8347EVAL QUADRATURE DEMODULATOR BOARD....21
B. EXPERIMENTAL SETUP....22
C. RESULTS AND ANALYSIS....25
D. SUMMARY....28

IV. WIRELESS LOCAL OSCILLATOR DISTRIBUTION....29
A. ANALOG DEVICES AD8346EVAL QUADRATURE MODULATOR BOARD....29
B. WIRED LO DISTRIBUTION....30
1. Experimental Set-up....30
2. Results....31
C. SIMULATION OF WIRELESS LO DISTRIBUTION....32
1. Multipaths Calculation....32
D. WIRELESS LO DEMONSTRATION....35
1. Experimental Set-up....35
2. Results....37
3. Further Investigation – Amplitude Variations....38
E. SUMMARY....41

V. DIGITIZATION AND SYNCHRONIZATION OF THE RECEIVE MODULES 43
A. NATIONAL INSTRUMENTS PXI-5112 DIGITIZER 43
B. DIGITIZATION OF RECEIVE MODULE 43
C. RESULTS AND ANALYSIS 45
1. Incorrect Gain Control in the Demodulator 47
2. Quantization Error of the NI5112 Digitizer 48
D. SYNCHRONIZATION OF THE RECEIVE MODULES 49
E. SUMMARY 50

VI. TRANSMISSION SYSTEM 51
A. TRANSMISSION SYSTEM 51
B. PARALLEL-PLATE TRANSMISSION SYSTEM 52
1. Transmission Loss Calculations 52
2. Cylindrical (Two-Dimensional) Propagation 55
3. Cylindrical and Spherical Propagation 57
C. SINGLE-PLATE TRANSMISSION SYSTEM 59
1. Analysis of Conducting Plane with Thin Dielectric Coating 59
2. Losses for Different Thickness and Dielectric Constant of the Dielectric Coating 61
D. SUMMARY 62

VII. CONCLUSION AND RECOMMENDATIONS 63
A. CONCLUSIONS 63
B. RECOMMENDATIONS FOR FUTURE WORK 63
1. Operational Amplifier in the Receive Module 63
2. Receive Antenna Hardware 64
3. Signal Processing 64
4. Transmission System 64

APPENDIX. MATLAB CODES 65
A. SIMULATION OF ARRAY FACTOR FOR N ELEMENT LINEAR ARRAY 65
B. PHASE RESPONSE OF AD8347EVAL DEMODULATOR 66
C. MODELING OF MULTIPATHS 67
D. AMPLITUDE VARIATION BETWEEN MODULATORS IN WIRELESS LO 69
E. TRANSMISSION LOSS IN PARALLEL PLATE TRANSMISSION 70
F. 2D AND 3D TRANSMISSION LOSS 71
G. SINGLE CONDUCTING PLANE WITH THIN DIELECTRIC FILM 72

LIST OF REFERENCES 75

INITIAL DISTRIBUTION LIST 77

LIST OF FIGURES

Figure 1. Major systems onboard the DDX (After [1]).....3
Figure 2. Geometry of a uniformly spaced linear array (After [4]). 8
Figure 3. Pattern of a 50-element linear phased array with a 30 deg scan angle. 10
Figure 4. Coupling between elements of an array (After Ref [5]). 11
Figure 5. Navy's proposed electric stealth destroyer, DD(X) (From [1]). 13
Figure 6. Simulation of an implementation of 1200 elements on the DD(X) (From [11]).....14
Figure 7. Block diagram of an opportunistic array architecture on a surface warship (From [9]).....15
Figure 8. Basic architecture of a transmit digital phased array. 16
Figure 9. Basic architecture of a receive digital phased array.....16
Figure 10. Wireless transmit/receive module architecture (From [11]). 17
Figure 11. In-phase and quadrature-phase demodulation (From [4]). 19
Figure 12. Block diagram of AD8347EVAL board (From Ref [10]). 22
Figure 13. AD8347EVAL demodulator board bench test. 22
Figure 14. AD8347EVAL board connections 23
Figure 15. Transmit and measured differential *I* and *Q* components. 26
Figure 16. Received and transmitted phase. 27
Figure 17. Phase errors between transmitted and received phases.....28
Figure 18. Functional block diagram of the AD8346EVAL quadrature modulator 30
Figure 19. Experimental set-up for a wired LO distribution. 31
Figure 20. Array output for wired LO distribution 32
Figure 21. Setup of computer simulation for wireless LO distribution.....33
Figure 22. Experimental set-up for wireless LO distribution. 35
Figure 23. External view of the absorbent box for wireless LO demonstration. 36
Figure 24. Setup of antennas in absorbing box for wireless LO demonstration. 36
Figure 25. Expected and measured array outputs of modulators with wireless LO distribution. 38
Figure 26. Amplitude variation in wireless LO distribution (0 deg phase difference). 40
Figure 27. Amplitude variation in wireless LO distribution (45 deg phase difference). ..41
Figure 28. Digitization of *I* and *Q* voltages. 44
Figure 29. NI5112 digitizer connections. 44
Figure 30. Customised LABVIEW software for digitization of receive modules. 45
Figure 31. Transmit phase versus receive phase. 46
Figure 32. Previously measured response between transmit and receive phase with AGC mode turned 'on' (From [3]). 47
Figure 33. Gain and linearity error of AD8347EVAL demodulator board (From [12])...48
Figure 34. Synchronization of two receive modules. 49
Figure 35. Connections of two AD8347EAVL demodulator boards. 50
Figure 36. Integrated ship transmission system (After [11] and [14]). 51
Figure 37. Propagation in a single-plate dielectric waveguide. 52

Figure 38. Transmission loss for parallel-plate dielectric with dielectric constant 2.0.....54
Figure 39. Cylindrical wavefront in parallel-plate transmission.....56
Figure 40. Phase plot of cylindrical wavefronts in parallel-plate waveguide. 56
Figure 41. MATLAB model for the two- and three-dimension propagation. 58
Figure 42. Power dissipation of two- and three-dimension propagation. 59
Figure 43. Conducting plane coated with thin layer of dielectric (After [14]). 60
Figure 44. Decay at $3\lambda_o$ and loss per meter for grounded dielectric slab with different dielectric constants and varying thickness.....61

LIST OF TABLES

Table 1. Results of the AD8347EVAL board bench test.....25
Table 2. Array outputs of modulators with wireless LO distribution. 37
Table 3. Amplitude variation of wireless LO at fixed 0 deg phase difference. 39
Table 4. Amplitude variation of wireless LO at fixed 90 deg phase difference. 40
Table 5. Phase inputs at modulator and outputs at demodulator. 46
Table 6. Power loss per unit length in dielectric.....55

THIS PAGE INTENTIONALLY LEFT BLANK

ACKNOWLEDGMENTS

I would like to express my gratitude to Professor David Jenn of the Naval Postgraduate School, Monterey, California for his guidance in this thesis work. His infinite patience, unflappable optimism and sense of humor are a great source of confidence and inspiration for all his thesis students. I would also like to thank Professor Donald Walters for agreeing to second-read the thesis and for his instructions and comments.

The work in this research would not have been possible without the assistance of the Bob Broadston, the laboratory director, and Sue Park, the Marketing Manager for National Instruments, both of whom I am deeply grateful. Finally, my time in NPS would have been much less enjoyable without the companionship of my fellow CST classmates: Mark, Mathew and Winston.

THIS PAGE INTENTIONALLY LEFT BLANK

I. INTRODUCTION

A. MOTIVATION

Information has always been at the center of a warfighter's preoccupation. What is the enemy doing? Where are his forces now? How can one know of an incoming threat? How can one maximize the response time to the threat? It is this preoccupation that combatants strive to improve their sensory capability to ensure survivability and mission success. A myriad of sensory capabilities are used by the military, such as radar, electro-optics and acoustics. However, no sensor can provide an extended range and at a relatively low cost compared to the radio frequency radar. It is for this reason that radar continues to remain the primary sensory capability for the military, as well as for the civilian industries.

Over the past decades, phased array radar has become the technology of choice in many civilian and military applications. Some of the important advantages of phased array systems are:

1. Agile and fast radar beam steering, as the beam steering is now done electronically rather than mechanically. Fast switching of beams can now be achieved.
2. Ability to track multiple targets, as the phased array radar is able to generate multiple independent beams at the same time.
3. Less mechanical components, which reduces the system footprint and increases the overall system availability.
4. Can be designed to conform to the shape of the platform, which would not adversely affect the aerodynamic or stealth characteristic of the platform.
5. Graceful degradation in performance, as redundancy is built into the multiple array elements.

For warships, the use of phased array radars makes possible the use of one system for air/surface detection, and another or the same system for fire control of multiple targets. The fire control function is the most important reason for the use of a phased array system, as phased array systems can redirect and steer radar beams fast enough to track multiple targets at any one time. Phased array radar systems can now

remove the sensory limitation out of the equation for modern warships. Warships are now capable of controlling more self-defense missiles than they can carry.

However, the competition for limited resources onboard the military platform remains unabated. Every system to be placed onboard the surface warship would require power, maintenance and most of all space. The larger the space used for the sensor system onboard the ship means a lesser number of weapons it can carry. Similarly, an additional infrastructure for the radar to be erected onboard the platform implies a compromise to its aerodynamic, maneuverability and stealth characteristics. For these reasons, innovative solutions need to be pursued to integrate the radar system into the next generation of warships.

The current AEGIS fleet, which is based on a conventional hull, is basically a design of a ship "around the radar". The ongoing endeavor for the next generation surface warship, the DD(X), is an attempt for a completely new surface ship design "from the ground up". The opportunistic array concept offers a revolutionary solution to the space constraint problem for the new-generation surface warship. The concept of an "aperstructure" with the integration of the opportunistic array into the hull or superstructure of the warship gives new radar capability to the warship. Figure 1 shows the aperstructure concept for the DD(X). The transmit/receive modules of the opportunistic array are integrated into available spaces of the ship's structure and hull. The beamforming data, control signals and target return signals are sent wirelessly between the transmit/receive modules and the beamformer and signal processor located away from the modules.

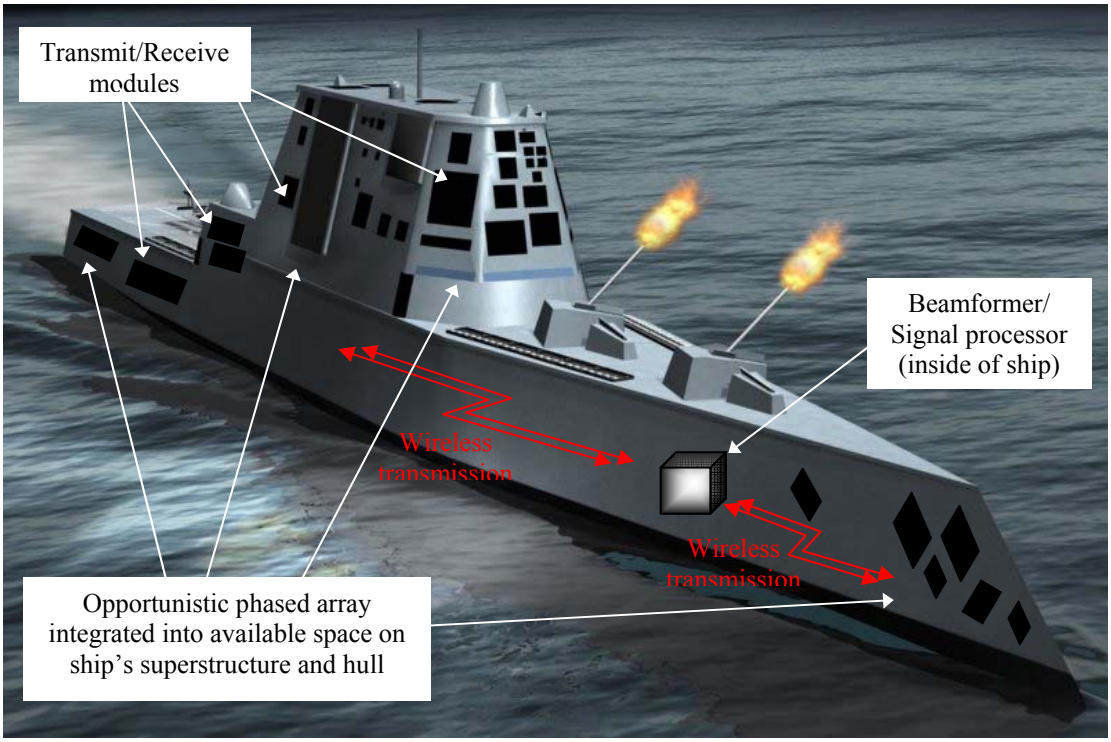

Figure 1. Major systems onboard the DDX (After [1]).

A primary purpose of the opportunistic array onboard the surface warship is ballistic missile defense (BMD). The mission for the opportunistic array is the exo-atmospheric surveillance, tracking, preliminary discrimination and designation (or handover) to a high precision tracking and identification radar. This research into opportunistic array is at the brink of a new chapter in radar application for the military.

B. PREVIOUS WORK

Work on the opportunistic digital phased array radar for surface warship started in [2] and continued in [3] and [4]. In [2], Genetic Algorithm (GA) was used to predict the behavior of an array antenna with randomly located elements. A three-dimensional 2.4 GHz test-bed phased array transmit antenna was constructed using commercial-off-the-shelf (COTS) products and the findings compared against the computer simulations. The test-bed antenna was constructed using the Analog Devices AD8346EVAL quadrature modulator boards, which were assembled into a

24-element array and configured as phase shifters. Each modulator fed one of the 24 printed circuit dipoles that acted as the radiating elements. The formation of the radiation beam and the radiation pattern was verified to be in agreement with the numerical simulations, thus demonstrating the viability of the transmit component of the phased array.

In [3], the research investigated the bandwidth characteristics of the AD8346EVAL modulator board. Another commercial product, the Analog Devices AD8347EVAL quadrature demodulator board was configured to operate as a phase shifter, and the phase response from the demodulator was measured and compared against the transmit phase from the modulator.

Reference [4] investigated the design of the complementary phased array receiver architecture centering around the AD8347 demodulator. The inappropriate operating conditions in [3] were corrected and a linear relationship between the received and transmitted phases of the demodulator and modulator board was demonstrated. To improve the phase distortion and increase the operating bandwidth of the phased array, [4] investigated the technique of using different types of time-varying phase weights for a linear frequency modulated signal on both the transmit and receive side.

C. SCOPE OF RESEARCH

The research in this thesis will continue the work performed in [2], [3] and [4]. The focus of this research is on the receive element of the phased array architecture. In the first part of the research, the bench test of the AD8347EVAL demodulator board conducted in [4] will be repeated to verify the linear relationship between the measured phase response from the AD8347EVAL with the transmitted phase from the AD8346EVAL modulator board.

The second part of the research will investigate the distribution of the local oscillator (LO) to two AD8346EVAL modulator boards in a wired and wireless setup. This is a necessary requirement for the coherent operation of the array elements. Results from this research prove the viability of a wireless local oscillator distribution

between the LO and the modulators for the array. The third part of the research involves the digitization and synchronization of multiple receive modules.

The final part of the research concerns the transmission system of the aperstructure. The wireless distribution of data and control signals between the digital beamformer and transmit/receive modules require a low-loss, wideband, simple to implement transmission system that is integrated into the structure of the warship. Two candidates for the transmission system will be investigated: a parallel-plate waveguide sandwiching a dielectric medium, and a single conducting plane with a thin dielectric film.

D. ORGANIZATION OF THESIS

The organization of this thesis broadly follows the scope of the research in sequence. Chapter II discusses the basic characteristics of the linear phased array, and gives an overview of conformal, thinned, and opportunistic arrays. The quadrature demodulation scheme and the architecture for the digital phased array transmit and receive configuration are also covered in this chapter. Chapter III contains the experimental work on the phase characteristics of the AD8347EVAL demodulator board. The experiments described in Chapter IV investigate the wired and wireless distribution of the local oscillator signals to a two-element transmit array (AD8346EVAL modulator boards). Chapter V contains the experimental work on the digitization of the receive modules for the conversion of the in-phase and quadrature-phase signals into phase readouts. Chapter VI covers the study of the two candidate transmission systems for the wireless data transfer. Finally, Chapter VII contains the summary of the results from the research and provides some recommendations for future follow-on work. All the MATLAB codes used in the research are contained in the Appendix.

THIS PAGE INTENTIONALLY LEFT BLANK

II. PHASED ARRAY RADAR AND DIGITAL ANTENNA ARCHITECTURE

This chapter discusses the basic characteristics of the linear phased array and provides an overview of the concept of conformal, thinned, and opportunistic arrays, which includes their challenges to radar designers. The quadrature demodulation scheme and the basic transmit and receive architecture for a digital phased array antenna are also discussed in this chapter.

A. LINEAR PHASED ARRAY

An array antenna is one where several separate antennas are arranged in space and interconnected to produce a directional radiation pattern [5]. Instead of a mechanical steering of the antenna, a phased array offers the capability of electronic scanning of the main beam. The array is called a phased array when scanning of the radiation beam is achieved by changes in the phase in the excitation of the individual antenna elements. When the array elements are lined up along an axis, it is called a linear phased array. A receive array is shown in Figure 2, but the following analysis also holds for a transmit array.

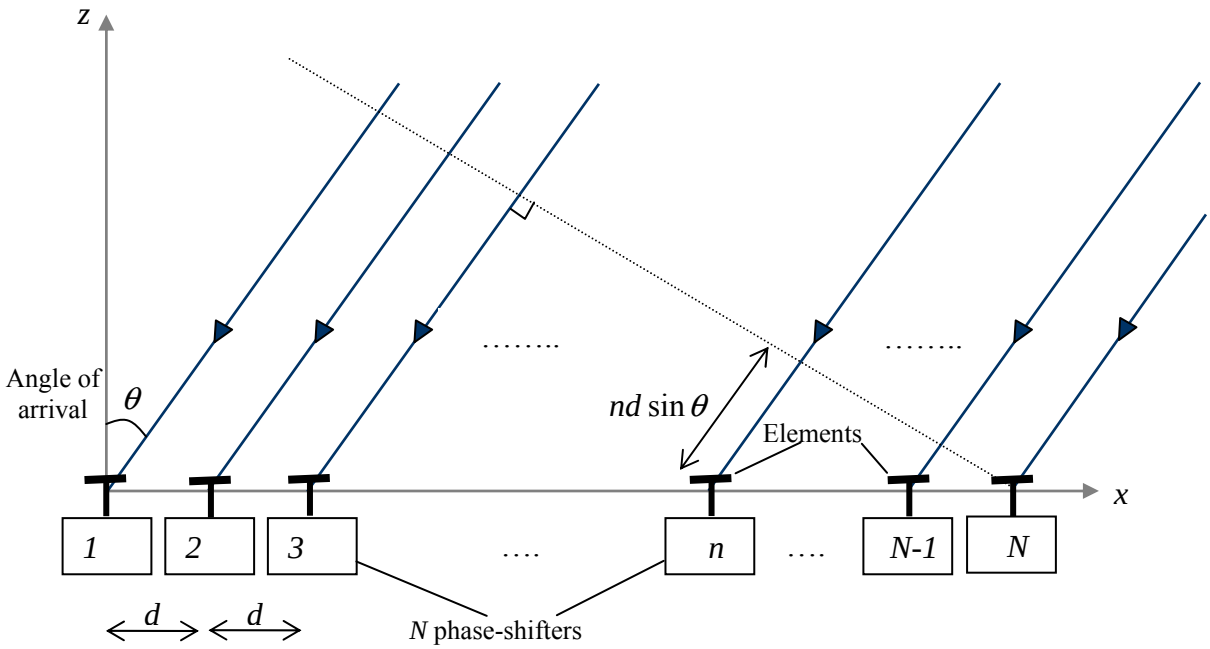

Figure 2. Geometry of a uniformly spaced linear array (After [4]).

1. Array Factor and Radiation Pattern

The radiation pattern of the phased array is the direct summation of the weighted response of the elements to an incident plane wave. This distribution of weights is called aperture distribution [6]. The array factor $AF(\theta)$ for a N-element array of uniformly-spaced array is given by [7]

$$AF(\theta) = \sum_{n=0}^{N-1} A_n e^{j\Phi_n} e^{-j\frac{2\pi}{\lambda} nd\sin(\theta)} \tag{2.1}$$

where N = number of elements

$A_n e^{j\Phi_n} = A_n e^{j\frac{2\pi}{\lambda} nd\sin(\theta_s)}$

= complex weights of the n^{th} element used to steer the beam in desired directions and control the sidelobes

θ_s = scanning direction of the main beam

d = spacing between elements

λ = wavelength

If it is assumed that all elements have the same radiation pattern, $EF(\theta)$, then the total pattern of the antenna $E(\theta)$ is the product of the array factor and the element pattern

$$E(\theta) = EF(\theta)AF(\theta) \tag{2.2}$$

The directivity D of the array can be computed from radiation pattern

$$D = \frac{4\pi \mid E(\theta) \mid^2_{\max}}{\int_0^{2\pi}\int_0^{\pi} \mid E(\theta) \mid^2 \sin\theta d\theta d\phi} \tag{2.3}$$

The array gain G is the directivity reduced by the array loss. If the array efficiency is

$$e = \frac{\text{Power out to the array}}{\text{Power collected by the array}} \tag{2.4}$$

then the array gain G is

$$G = eD \tag{2.5}$$

Figure 3 shows the radiation patterns produced by a 50-element linear phased array with uniform amplitude at 2.4 GHz and a 30 deg scan angle. The element spacing is set at half the wavelength of the frequency 2.4 GHz. The main beam peak is at 30 degrees. There are $N-2$ sidelobes in the pattern with the highest one about 13.2 dB below the peak of the main beam. It can be observed from the plot that the sidelobes are not symmetrical about the main beam.

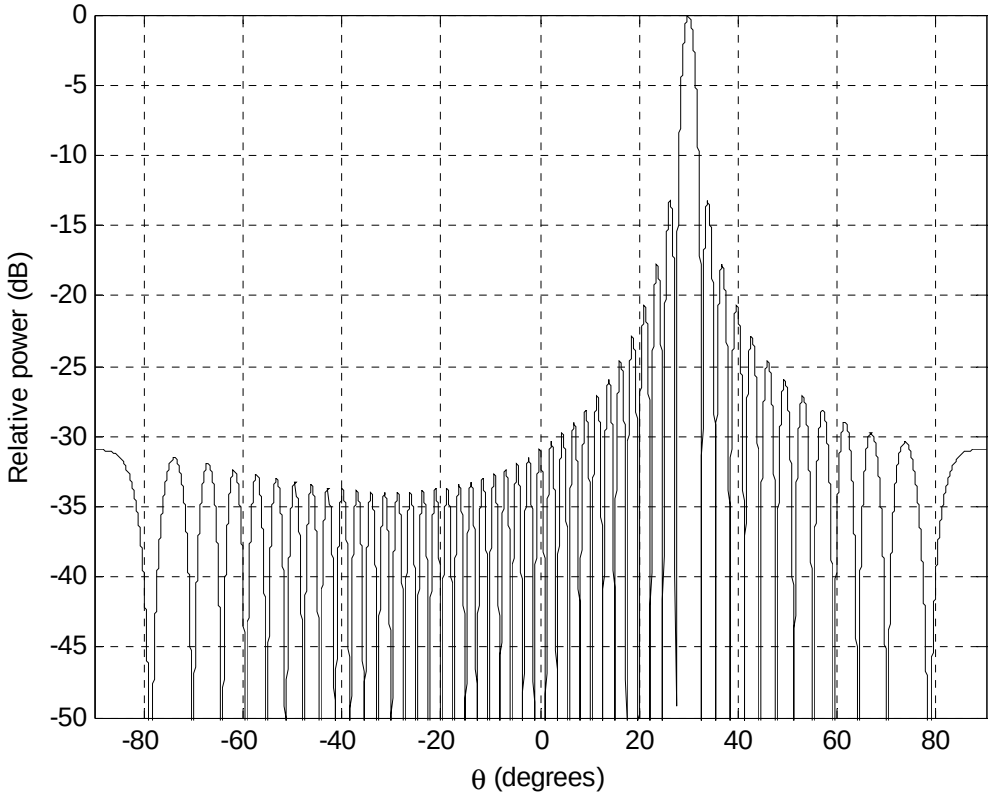

Figure 3. Pattern of a 50-element linear phased array with a 30 deg scan angle.

While phased arrays offer many advantages over aperture antennas, they also present a number of challenges to the radar system design. Two of these challenges are bandwidth limitations and mutual coupling.

2. Bandwidth Limitations

To account for the radiation pattern as a function of radiating frequency and phase in wideband operation, Equation (2.1) is expressed in terms of frequency f instead of wavelength λ to give:

$$AF(f,\theta) = \sum_{n=0}^{N-1} A_n(f) e^{j\frac{2\pi f}{c} nd\sin(\theta_s)} e^{-j\frac{2\pi f}{c} nd\sin(\theta)} \tag{2.6}$$

Bandwidth limitation of the array arises when the position of the main beam changes with frequency. To keep the beam position fixed, the first exponential ($e^{j\frac{2\pi f}{c} nd\sin(\theta_s)}$) in Equation (2.6) must change with frequency in the same way as the

second exponential ($e^{-j\frac{2\pi f}{c}nd\sin(\theta)}$) [3]. This can be accomplished using a true time delay phase shifter or time varying phase shift.

3. Mutual Coupling between Elements

The presence of the surrounding environment changes the current distribution (and thus impedance) of each element, and the field collected by each element is dependent on the induced currents on the other elements as well as its own [8]. The radiation pattern of each array element could therefore be altered in magnitude and phase as a result of the mutual coupling with nearby elements, as compared to an isolated element. In addition, these effects are dependent on frequency and scan direction of the element. For an array in a receive mode, the resultant pattern at the individual element would have both a dominant component due to the direct incident plane wave, as well as the less dominant contributions due to scattering of the incident wave at neighboring elements.

A schematic diagram of mutual coupling is given in Figure 4. As a result of mutual coupling, the patterns of the elements are not identical and the element factor in Equation (2.1) cannot be factored out of the sum. For a conventional periodic array, the mutual coupling is the same for all elements, except for the few around the edges. Since this is often a relatively small number compared to the total, identical element patterns can be assumed. In the case of an opportunistic array, the elements are randomly located and therefore identical pattern cannot be assumed.

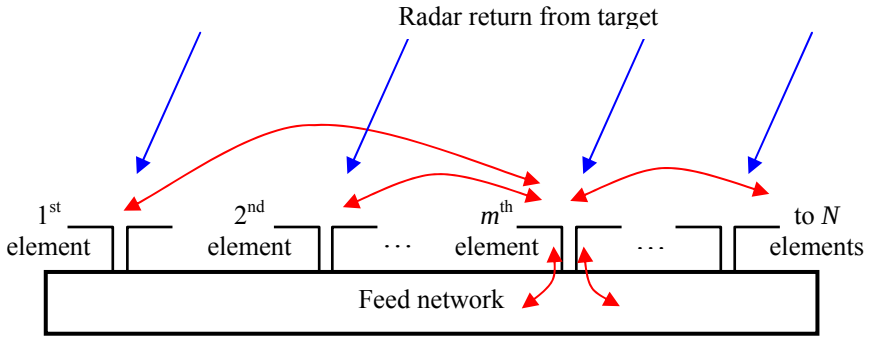

Figure 4. Coupling between elements of an array (After Ref [5]).

B. MULTI-DIMENSIONAL AND CONFORMAL ARRAY CONCEPT

In addition to a linear or planar array where the elements are lined up in a straight line or on a plane, another emerging class of a phased array has the element locations conform to a non-planar surface. This type of array is in the class of multi-dimensional arrays and called a conformal array. Conformal arrays have promising applications for the military where the arrays can be implemented on the skin of a military vehicle or on the nose, wings or fuselage of an aircraft. However, it is not an easy task to achieve a practical conformal array with complicated geometry. Challenges arise in non-planar surfaces when the element polarization and beam pointing direction varies from one element to another, or when the aperture illumination cannot be separated into two orthogonal patterns [9]. However, these types of problems can be easily handled by digital antennas, because corrections can be applied to the array data before it is processed.

C. THINNED ARRAY – APERIODIC AND RANDOM

The elements of a regular periodic phased array are usually spaced about a half-wavelength apart for optimum performance. Thinned arrays refer to those whose elements are spaced, on average, more than half-wavelength from each another. This can be achieved either by turning some elements off or more often, physically removing them. This preserves the beamwidth of the array as if it were completely filled, but the gain is reduced and the sidelobes increase. If the array spacings are selected by a deterministic algorithm, the array is said to be aperiodic. Otherwise, if the spacings are randomized, it would be called a random thinned array [6, 9].

For an aperiodic spacing of the elements, the Genetic Algorithm (GA) is one of several methods to determine the element weights that would result in an acceptable antenna pattern. Via the GA, the antenna patterns for a fixed number of elements can be calculated from all the possible element locations, and the best combination determined. The pattern may be found using all elements or just some. They may or may not be equally weighted in amplitude and phase. The GA determines the best combination given a “fitness” function. Another method is called density tapering. In density taper, the density of equal-amplitude elements is made to

approximate the desired aperture illumination, and the choice to whether or not include an element in a possible location may be statistically or deterministically determined [9].

D. OPPORTUNISTIC ARRAY CONCEPT

An opportunistic array falls into the category of thinned or random array, where the array elements are placed at available and suitable areas of the overall infrastructure or platform. In a surface warship application, the opportunistic array elements would be placed at available open areas over the entire length (or surfaces) of the ship. The opportunistic digital phased array would be integrated into the ship structure as an aperstucture. The aperstructure would retain the stealth characteristics of the warship, as well as maximize its survivability and maneuverability. Figure 5 shows the Navy's proposed new generation electric stealth destroyer, the DD(X). An opportunistic array concept can be implemented on available ship structures and surfaces, as shown in Figure 6, with a total 1200 elements. The primary function of the array shown in Figure 5 is Ballistic Missile Defense (BMD). The simulation of the beam pattern in Figure 6 was with 620 active elements at 15 deg elevation cut. A preliminary system study has led to the selection of the 200 to 400 MHz frequency band [10]. The simulation shown is at f = 300 MHz.

Figure 5. Navy's proposed electric stealth destroyer, DD(X) (From [1]).

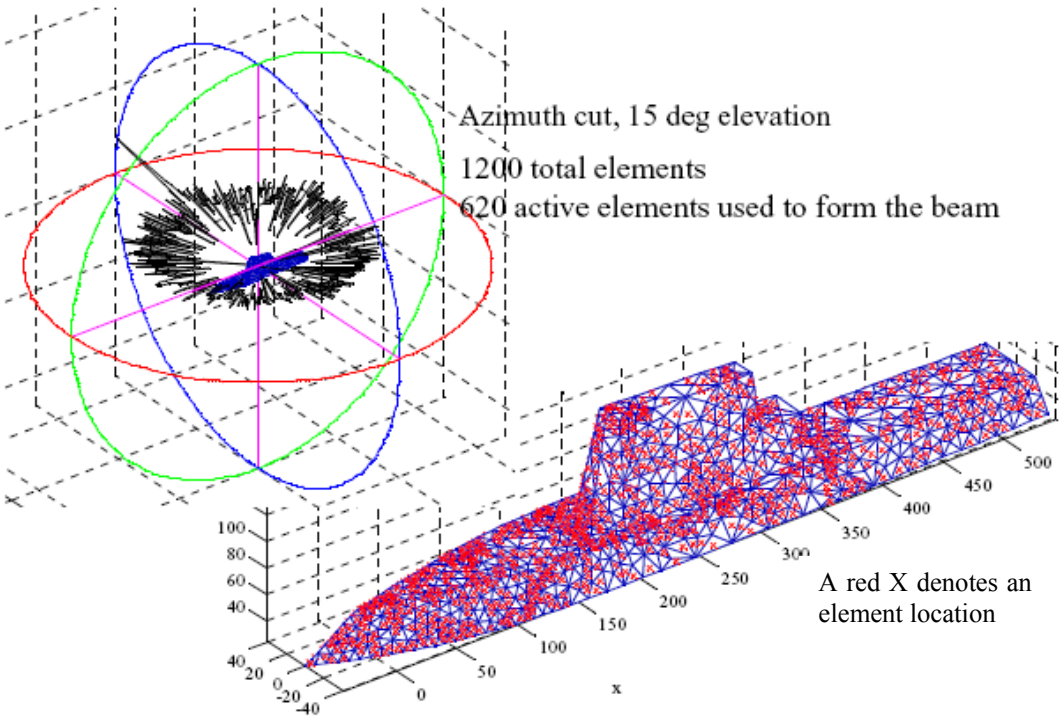

Figure 6. Simulation of an implementation of 1200 elements on the DD(X) (From [11]).

A block diagram of an integration of an opportunistic array into a surface warship is shown in Figure 7. The elements of the opportunistic array are self-standing transmit/receive (T/R) modules that have no hardwire connections other than prime power. Without the hardwire connections, synchronization signals, beam control data, and digitized radar signals are passed wirelessly between the elements and a central processing unit located below deck or at a less-demanded part of the ship. The unique feature of this design is therefore the wireless distribution and collection of the radar signal data and synchronization signals.

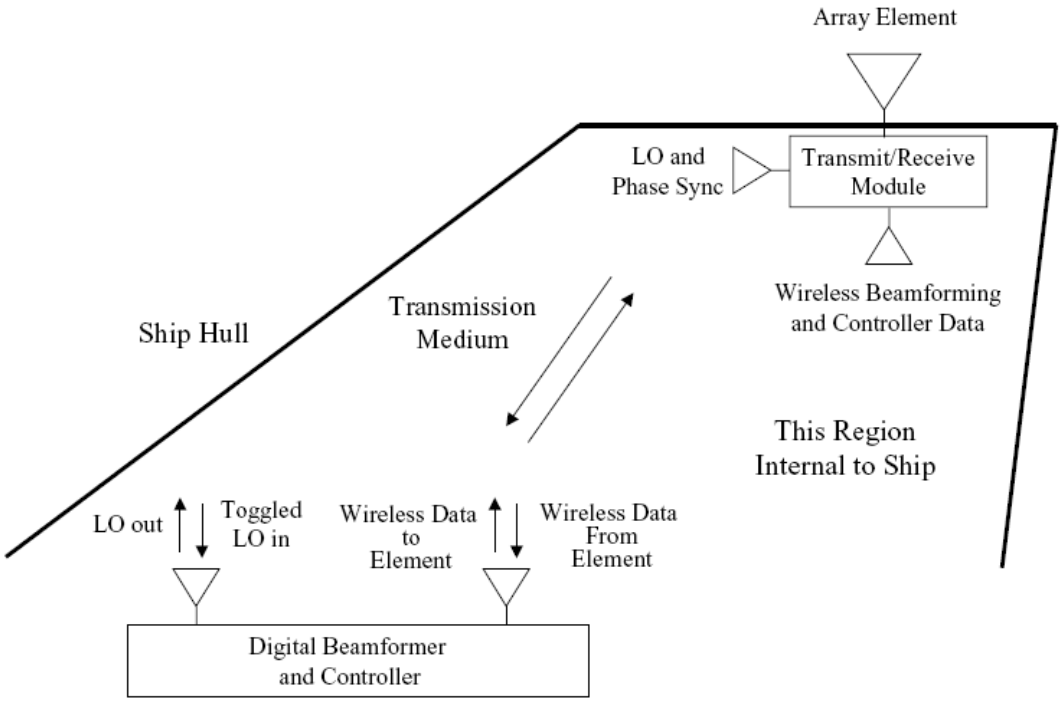

Figure 7. Block diagram of an opportunistic array architecture on a surface warship (From [9]).

E. DIGITAL ANTENNA ARCHITECTURE

The basic architectures of a digital phased array transmit module is shown in Figure 8. The broad sequence of operation in the transmit module works as follows. The Digital Beamformer and Controller provides the beamforming data and radar waveform in digital format to the Digital-to-Analog Converter (DAC), which converts it into the analog format suitable for modulation. The quadrature modulator works as a phase shifter and amplitude controller and modulates the analog data with the carrier signal supplied by the local oscillator (LO). The final phased shifted signals are then fed to the multiple array elements for transmission.

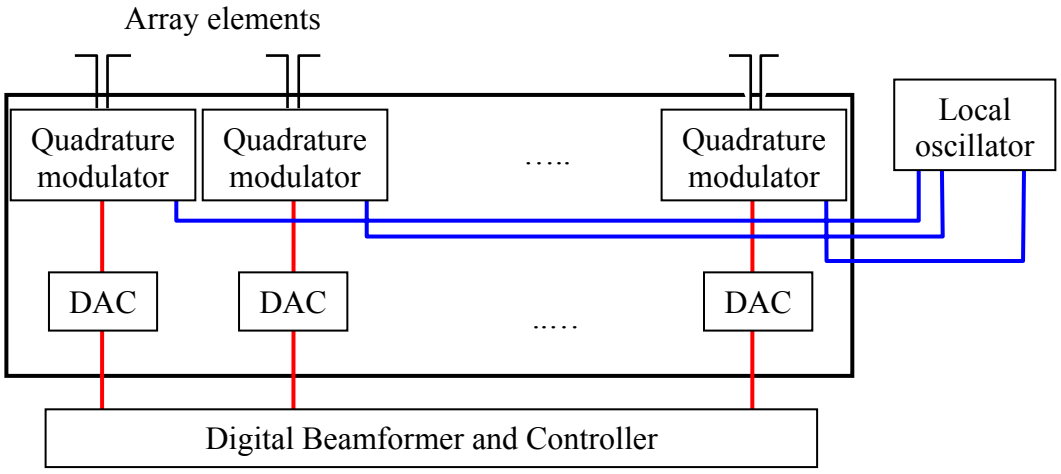

Figure 8. Basic architecture of a transmit digital phased array.

Figure 9 shows the basic architectures of a digital phased array receiver. The operation of the receive phased array is in reverse order of the transmit module. The signal returned from the target is first received by the various array elements. The data is down converted to baseband using the carrier signal provided by the LO. The resultant signal, still in its analog form, is converted into digital format by the Analog-to-Digital Converters (ADC). The final digitized signal is then passed to the Digital Signal Processor (DSP) for processing and target data extraction.

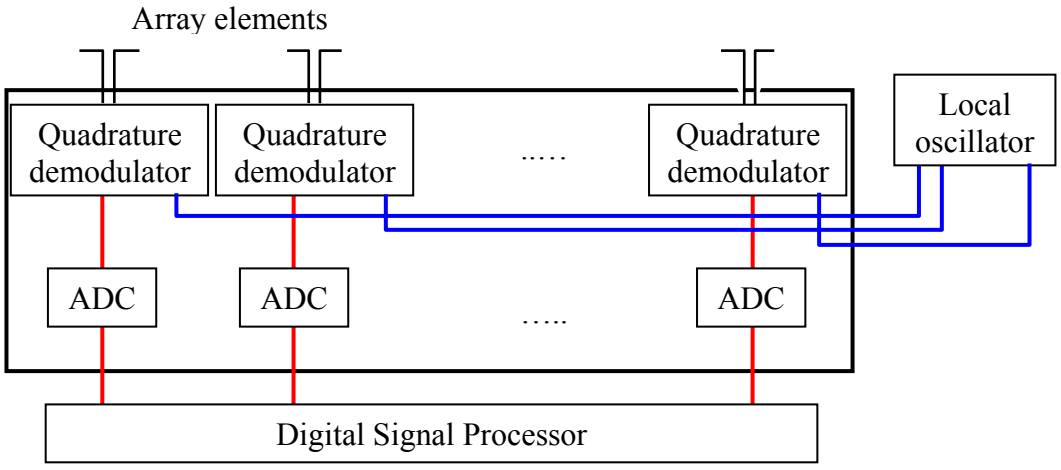

Figure 9. Basic architecture of a receive digital phased array.

The digital architecture for an array has many advantages. Advanced signal processing techniques can be applied to the data. Other radar, direction-finding and communication functions can be handled by the array as well. The conformal, dispersed element opportunistic array concept allows the possibility of economic retrofits and the benefits of redundancy due to attrition. The concept therefore has the advantages of large numbers and provides for quicker deployment, wider coverage, and more flexibility than a single-radar ship. In principle, the approach can be applied to combatants and as well as the auxiliaries. The concept is well suited to the "aperstructure" philosophy, where the array is now an integrated part of the ship structure.

F. WIRELESS LO DISTRIBUTION FOR DIGITAL ANTENNA CONCEPT

From the above basic architectures of the phased array transmitter and receiver, an integrated transmit/receive module, complete with a wireless distribution for the LO and beamforming data, can be drawn up. This is shown in Figure 10, where the transmit and receive function for each element are combined in a transmit/receive (T/R) module. Also, the wired connections between the LO and signal processor have been replaced by wireless links.

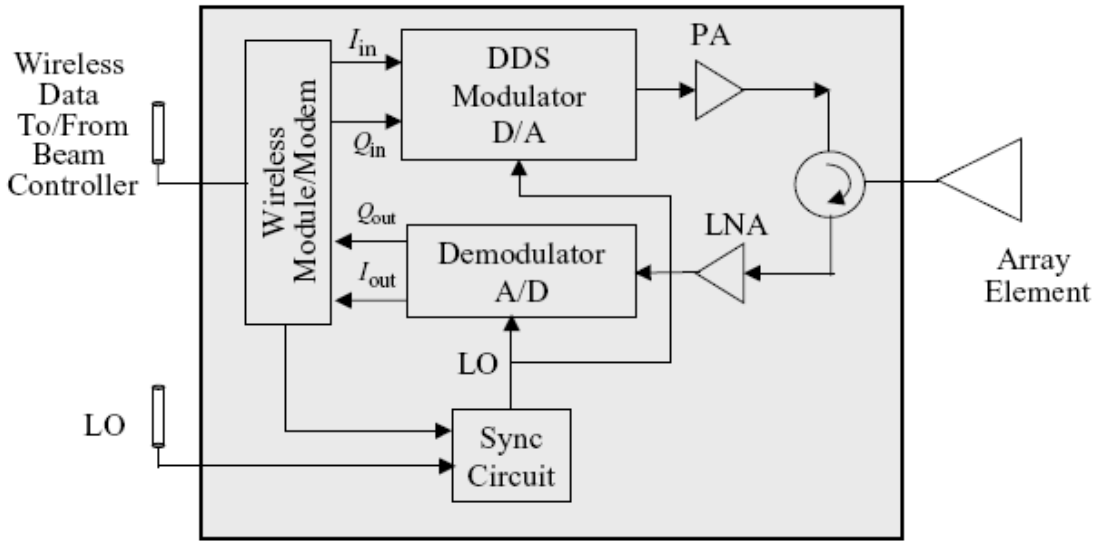

Figure 10. Wireless transmit/receive module architecture (From [11]).

The reference LO signal is distributed to both the modulator and demodulator wirelessly, and a "beam tagging" algorithm is used to dynamically synchronize all of the elements to a reference. The hardware required is contained in the "Sync Circuit". It corrects for errors in the element locations due to ship surface distortion and propagation changes in the wireless channel. The transmit waveform data is also transferred wirelessly between the T/R module and the beamformer. The signal is modulated and power amplified before being sent to the array element for transmission. On receive, the process is reversed, where the radar echo is demodulated after low-noise amplification (LNA), and the in- and quadrature-phase data is returned to the signal processor via the wireless channel [11].

G. QUADRATURE DEMODULATION SCHEME

After the received signal is converted to a baseband signal, it will be demodulated into the in-phase (I) and quadrature-phase (Q) terms. For a narrowband signal, this would be of the form

$$s(t) = A(t)\cos[\omega_c t + \Phi(t)] = I(t)\cos(\omega_c t) - Q(t)\sin(\omega_c t) \tag{2.7}$$

where $I(t) = A(t)\cos(\Phi(t))$ is the in-phase component of $s(t)$

$Q(t) = A(t)\sin(\Phi(t))$ is the quadrature-phase component of $s(t)$

$A(t)$ = Amplitude of $s(t)$

$\Phi(t)$ = Phase of $s(t)$

$\omega_c = 2\pi f_c$ is the angular frequency

f_c = Carrier frequency

In the demodulation scheme, the amplitude and phase of the receive signal can then be recovered from the in- and quadrature-phase components using

$$A(t) = \sqrt{I(t)^2 + Q(t)^2} \tag{2.8}$$

$$\Phi(t) = \tan^{-1}\frac{Q(t)}{I(t)} \tag{2.9}$$

This is conventionally illustrated in the I-Q plane shown in Figure 11. Figure 11 also shows an *I* and *Q* demodulation scheme where the local oscillator frequency is set to be equal to the carrier frequency, so as to produce a baseband signal. This kind of architecture is called homodyne or direct conversion detection.

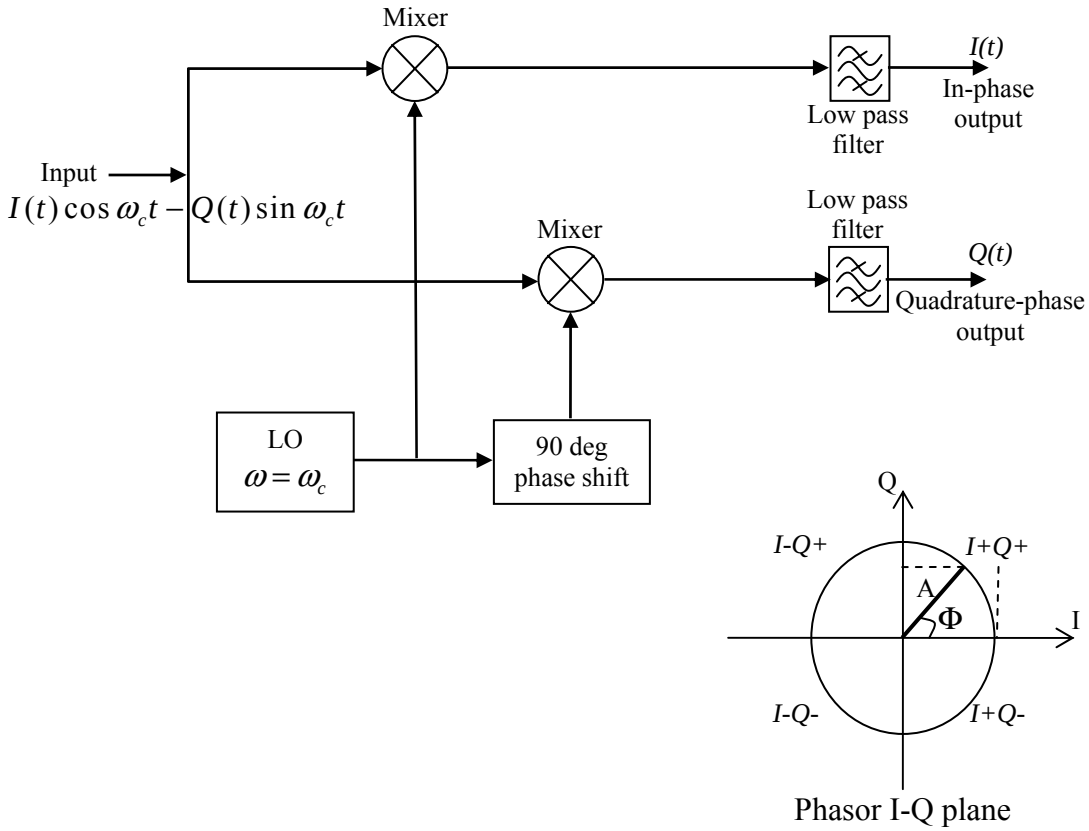

Figure 11. In-phase and quadrature-phase demodulation (From [4]).

H. FREQUENCY SELECTION

Based on the preliminary system study of the opportunistic array, the 200-400 MHz frequency band will be used for the carrier frequency, i.e., $200 \le f_c \le 400$ MHz. However, for the concept validation and demonstration, 2.4 GHz will be used due to the wide selection of low cost commercial products operating in this frequency band. The wireless data links, with the exception of the LO, can operate at a frequency independent of the carrier.

I. SUMMARY

This chapter discussed the basic characteristics of the linear phased array and gave an overview of the concept of conformal, thinned and opportunistic radar. The basic architecture of the transmit and receive module of the phased array was also discussed in this chapter. The next few chapters will report on the measurements of the research, starting with the phase characteristics of the demodulator and the wireless distribution of the local oscillator signals.

III. PHASE CHARACTERISTICS OF QUADRATURE DEMODULATOR

The option of using commercial-off-the-shelf I/Q demodulator boards as phase shifters was proposed in [3], where each phased array element is connected to a demodulator and then converted to digital format with an ADC. The ADC is in turn connected to a low-cost Input/Output (I/O) board of the signal processor. In this case, the signal processor is a PC running the LABVIEW program. The demodulator board chosen was the Analog Devices AD8347EVAL board. The investigation of the board's characteristics in [4] was verified and expanded in this chapter.

A. ANALOG DEVICES AD8347EVAL QUADRATURE DEMODULATOR BOARD

The AD8347EVAL demodulator board is a broadband direct quadrature demodulator with RF and baseband Automatic Gain Control (AGC) amplifiers, which perform quadrature demodulation directly to baseband frequencies. The input frequency range of the board ranges from 0.8 to 2.7 GHz. To ensure complete compatibility, the AD8347EVAL demodulator board on the receive end is used together with the AD8346EVAL modulator board on the transmit end [12].

The AD8347EVAL demodulator board directly down-converts the RF signal to *I* and *Q* baseband components after mixing with the LO signal. The *I* and *Q* voltage outputs are measured at the in-phase output positive (IOPP), in-phase output negative (IOPN), quadrature-phase output positive (QOPP), quadrature-phase output negative (QOPN), as shown in Figure 12.

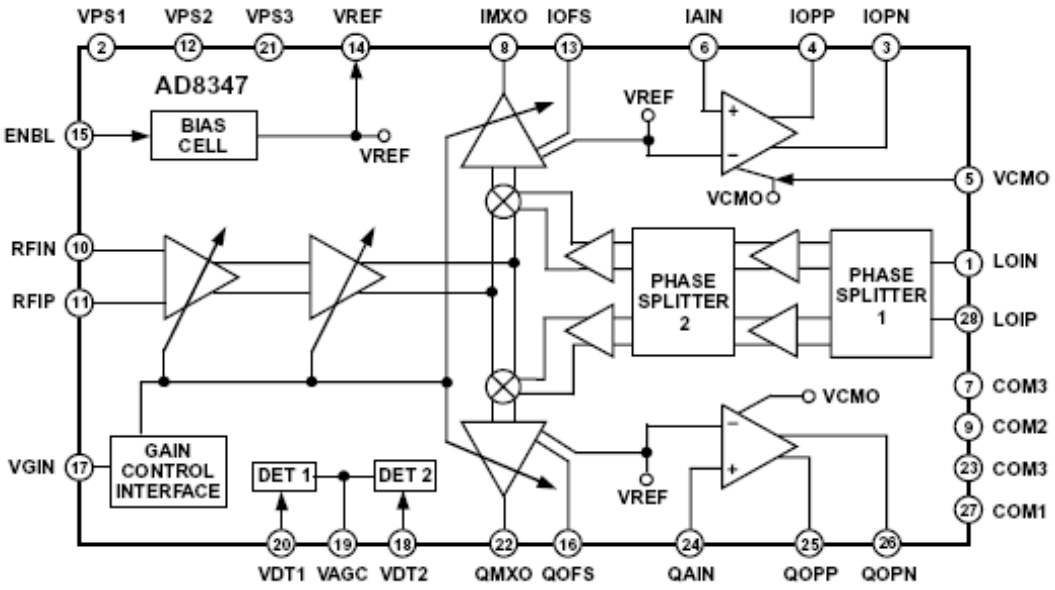

Figure 12. Block diagram of AD8347EVAL board (From Ref [10]).

B. EXPERIMENTAL SETUP

A schematic setup for the phase response measurement of the AD8347EVAL demodulator board is shown in Figure 13. Four voltmeters were used to read the *I* and *Q* voltages from the AD8347EVAL demodulator board. The phase of the signal is subsequently calculated from these *I* and *Q* voltages using Equation (2.9).

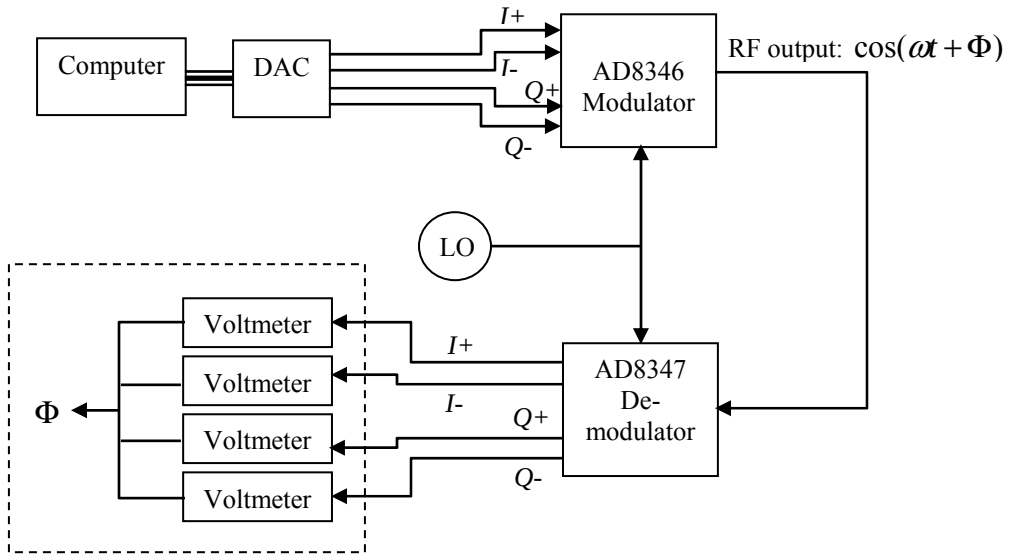

Figure 13. AD8347EVAL demodulator board bench test.

The connections for the bench test of the AD8347EVAL board are shown in Figure 14. A 5V DC voltage from an external power supply was used to power up the AD8347EVAL board. The +5V and ground connection were connected to the "VS" and GND" pins on the AD8347EVAL board. The location of the power On/Off switch is also shown in Figure 14.

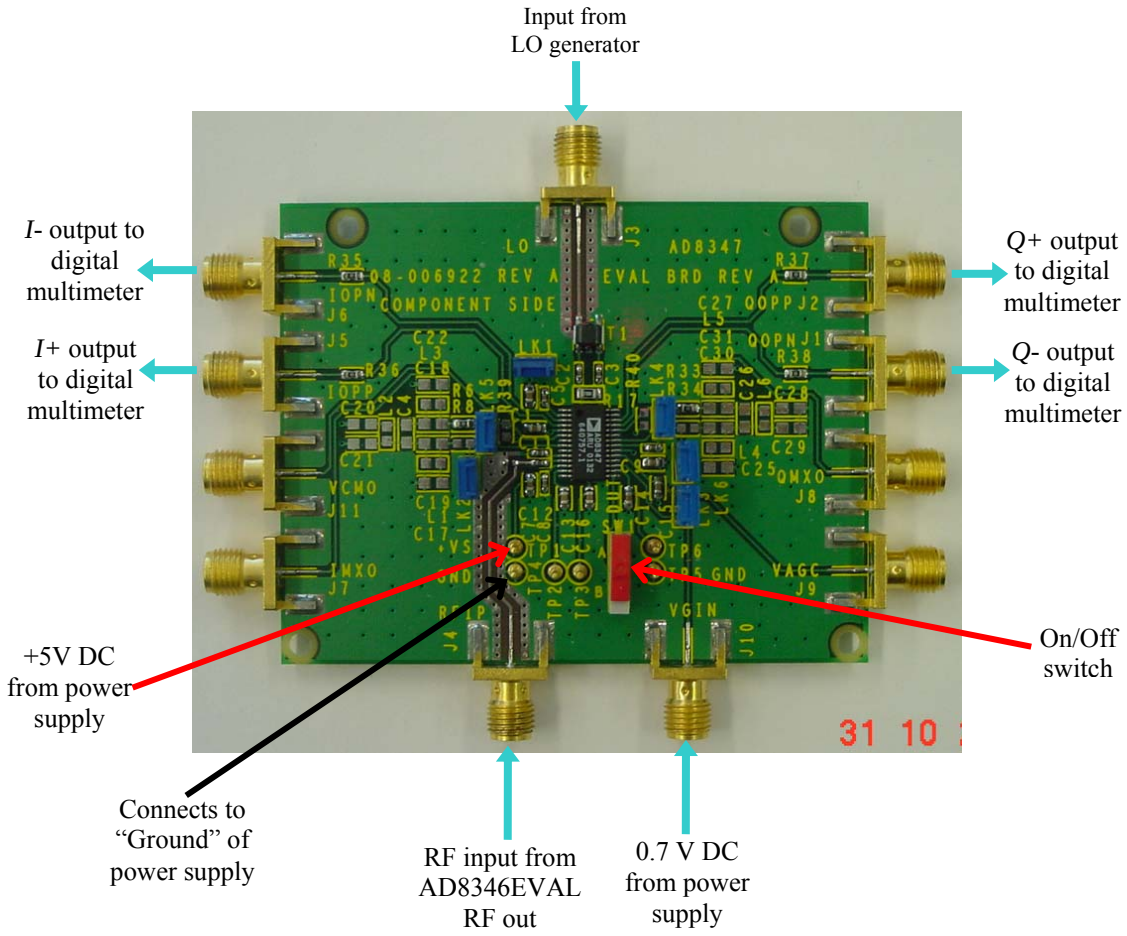

Figure 14. AD8347EVAL board connections

The LO input for the AD8347EVAL board was drawn from the same LO generator as that for the AD8346EVAL board. A power splitter and equal length cables from the power splitter to the two boards ensured that the received RF signal at the AD8347EVAL board was perfectly synchronized with the LO signal at the AD8346EVAL board. The LO generator operated at 2.4 GHz was within the specified range (0.8 to 2.7 GHz) of the AD8346/7EVAL boards. According to the

product data sheet [9], the LO drive level for the AD8347EVAL board should be between -10 and 0 dBm, with -8 dBm being the recommended level. Accordingly, a RF attenuator (total of 37 dB) was required to ensure the appropriate strength of the LO input going into the AD8347EVAL board.

The RF and baseband amplifiers of the AD8347EVAL board would together provide 69.5 dB of gain control, with a precision control circuit in the board setting the linear-in-dB RF gain response to the gain control voltage. Although the AD8347EVAL board was capable of automatic gain control, this was not used, as it would result in phase errors in the I-Q outputs [3]. Instead, a fixed voltage was applied at the gain control input (VGIN) to control the gain on the RF and baseband variable gain amplifiers (VGAs). The range of the user-input gain control voltage on the AD8347EVAL board was 0.2 to 1.2 V, which corresponded to a gain range of +39.5 dB to -30 dB. (The additional 30 dB of gain was in the baseband amplifier). This gain control function at the VGIN input had a negative sense in that the increase in the control voltages decreased the gain and vice versa. A voltage of 0.7 V was used as the fixed gain control voltage in the experiment. The automatic gain control function of the AD8347EVAL board was disabled, i.e., not connected. Finally, it should be noted that setting the fixed gain too high, i.e., too low VGIN input (0.4 V), would result in saturation and give noisy readings.

LABVIEW control software was used to generate the amplitude and phase of the RF output of the AD8346EVAL board. The amplitude was set at '1' and the phase was set from 0 to 350 deg at 10 deg increments. The RF output from the AD8346EVAL board was connected directly to the "RFIP" input on the AD8347EVAL board. Finally, the quadrature outputs, '*I*+' (IOPP), '*I*-' (IOPN), '*Q*+' (QOPP) and '*Q*-' (QOPN), from the AD8347EVAL board were measured with respect to ground using four digital multimeters. To ensure accurate readings, all connections must be properly tightened and the correct power-up sequence of the devices and the LABVIEW software adhered to.

C. RESULTS AND ANALYSIS

Voltage readings were taken from the IOPP, IOPN, QOPP and QOPN off four digital multimeters for phases of the RF input at the AD8346EVAL board from 0 to 350 deg in 10 deg increment. The readings were taken to 1 mV in significant values. The amplitude and offset of the RF input were set at 1 and 0 deg respectively. The results obtained are tabulated as Table 1.

Transmit Phase (deg)	IOPP (VDC)	IOPN (VDC)	QOPP (VDC)	QOPN (VDC)
0	0.9979	1.0377	1.0226	1.0109
10	0.999	1.0367	1.0233	1.0102
20	0.9998	1.0358	1.0241	1.0094
30	1.0005	1.0352	1.025	1.0086
40	1.0011	1.0346	1.0259	1.0077
50	1.0014	1.0342	1.0269	1.0067
60	1.0016	1.034	1.0279	1.0058
70	1.0016	1.0341	1.0288	1.0048
80	1.0013	1.0343	1.0298	1.0039
90	1.0007	1.035	1.0307	1.003
100	0.9998	1.0359	1.0316	1.0022
110	0.9989	1.0368	1.0323	1.0014
120	0.998	1.0377	1.0331	1.0007
130	0.9971	1.0386	1.0336	1.0002
140	0.9961	1.0396	1.034	0.9998
150	0.9951	1.0406	1.0342	0.9996
160	0.9941	1.0416	1.0342	0.9996
170	0.9932	1.0426	1.0339	0.9999
180	0.9923	1.0435	1.0333	1.0005
190	0.9914	1.0444	1.0324	1.0014
200	0.9907	1.0452	1.0315	1.0022
210	0.9899	1.0459	1.0306	1.0031
220	0.9894	1.0464	1.0297	1.004
230	0.989	1.0468	1.0287	1.0049
240	0.9889	1.047	1.0278	1.0058
250	0.9889	1.0469	1.0268	1.0068
260	0.9892	1.0466	1.0258	1.0077
270	0.9899	1.0459	1.0249	1.0086
280	0.9908	1.045	1.0241	1.0094
290	0.9917	1.0441	1.0233	1.0102
300	0.9926	1.0431	1.0226	1.0108
310	0.9936	1.0422	1.0221	1.0114
320	0.9946	1.0412	1.0217	1.0118
330	0.9956	1.0402	1.0215	1.012
340	0.9966	1.0392	1.0215	1.0119
350	0.9975	1.0382	1.0218	1.0117

Table 1. Results of the AD8347EVAL board bench test

With the readings, the differential *I* and *Q* voltages were calculated by taking the differences (IOPP – IOPN) and (QOPP – QOPN) respectively. The received phase of the baseband signal was then calculated using Equation (2.9)

Figure 15 shows the measured differential *I* and *Q* component versus the transmit phase (sinusoidal waveforms) from the modulator. From the plots, the agreement is good between the transmit phase waveform and that of the measured *I* and *Q* components. Ideally, the waveforms of the measured differential *I* and *Q* components should be identical to the transmitted waveforms.

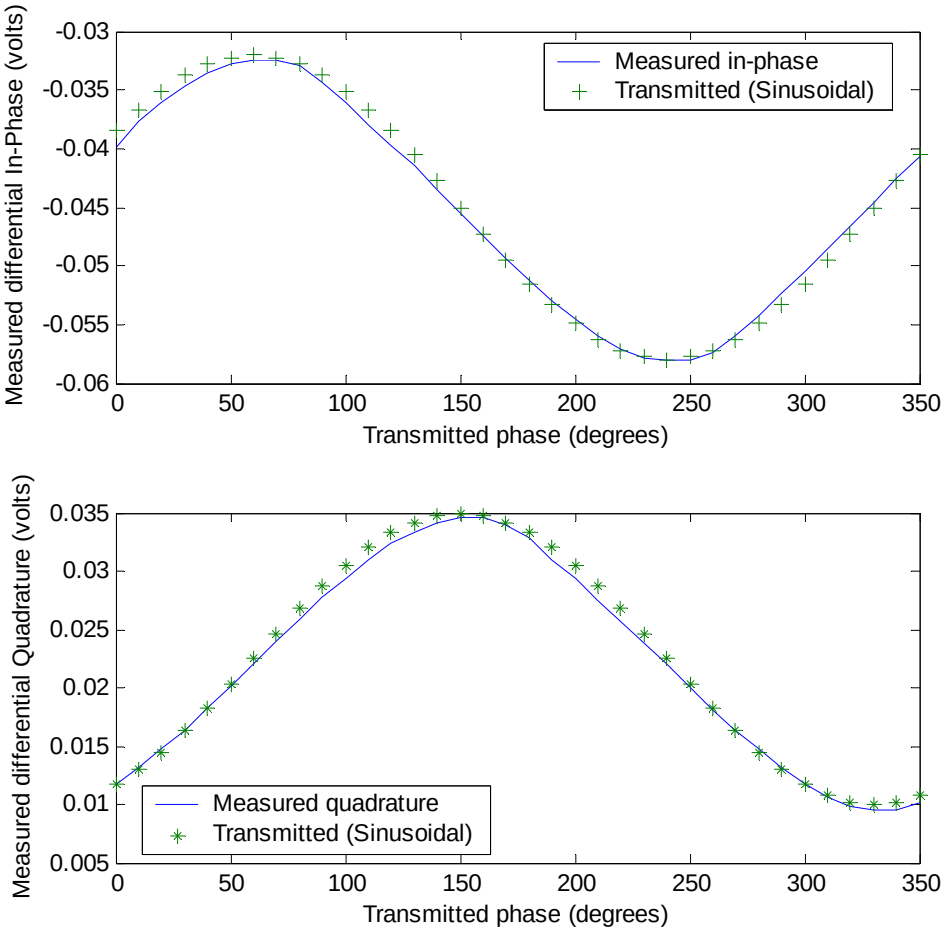

Figure 15. Transmit and measured differential *I* and *Q* components.

Figure 16 plots the transmitted and received phase on common axes. As with the results in Reference [3], the plots show that the transmitted and received phases are almost identical with no huge phase difference between the two. The small phase errors between the transmitted and received phase are plotted in Figure 17, where it shows the a largest peak phase error of only about 5.8 deg at around 320 deg transmitted phase. The root-mean-square (rms) phase error for the entire range is 1.7657 deg. These errors are considered negligible and are attributed to environmental and measurement errors. The bench test successfully demonstrated the suitability of the AD8347EVAL board to be used as a demodulator capable of accurately receiving the transmitted phase.

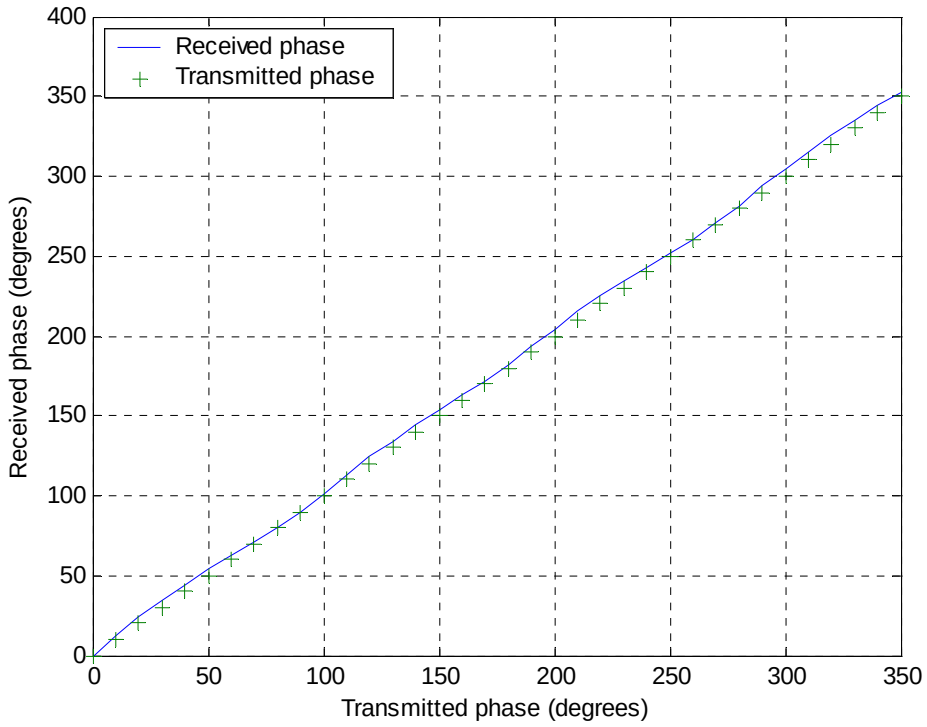

Figure 16. Received and transmitted phase.

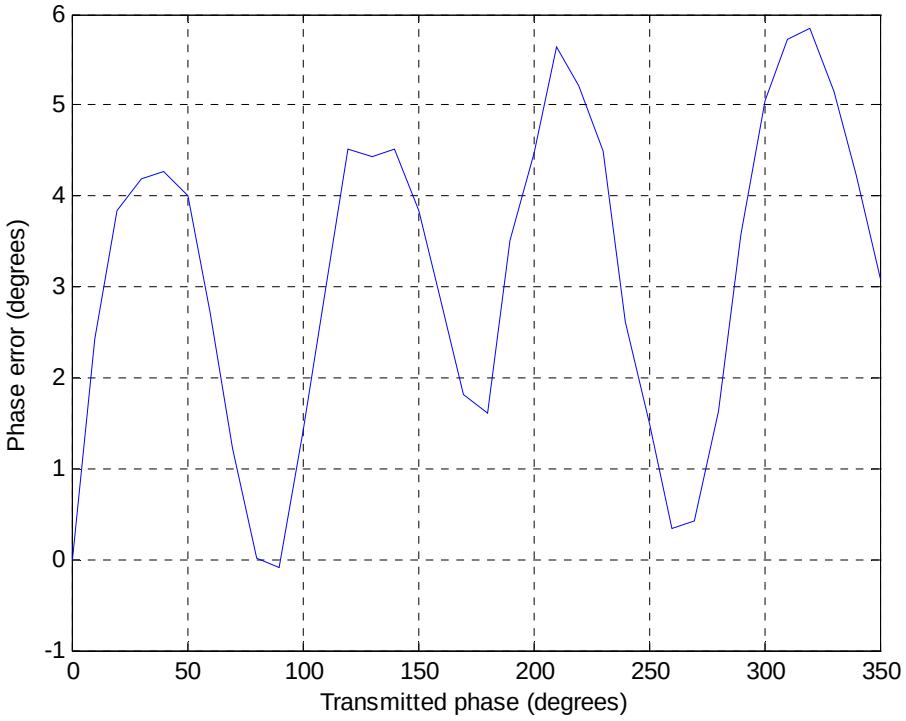

Figure 17. Phase errors between transmitted and received phases.

D. SUMMARY

This chapter discussed the phase characteristics of the AD8347EVAL demodulator board. The bench test demonstrated the linear response between the receive and transmit phase with the appropriate gain setting on the demodulator board. The bench test proved the suitability of the AD8437EVAL as the demodulator of the RF input in the receive module. The experimental setup used in the bench test of the AD8347EVAL demodulator board is also used in the next chapter on the wireless LO distribution.

IV. WIRELESS LOCAL OSCILLATOR DISTRIBUTION

Elements of an opportunistic phased array onboard the surface warship would be placed at random and available spaces at the topdeck of the ship's infrastructure. With some 1200 elements expected, a conventional wired set-up for the arrays would not be feasible. This section investigates the feasibility of a wireless distribution of the LO signal as the first step to a wireless implementation of the opportunistic phased array. Baseline results will first be determined from a wired LO distribution setup and propagation simulations of the wireless LO set-up. The results from these will be used to evaluate the wireless LO results.

A. ANALOG DEVICES AD8346EVAL QUADRATURE MODULATOR BOARD

The AD8346EVAL board is a silicon RF Integrated Circuit (RFIC) I/Q modulator for use in the 0.8 to 2.5 GHz frequency range. The quadrature modulator can be used as the transmit modulator in digital systems such as Personal Communications Services (PCS), Global Satellite Mobile (GSM) and Code Division Multiple Access (CDMA) transceivers. The board can be used with direct digital synthesizers in hybrid phase-locked loops to generate signals over a wide frequency range with mHz resolution. Its excellent phase accuracy and amplitude balance allow high performance direct modulation to RF. The baseband quadrature inputs are directly modulated by the LO signal to produce various Quadrature Phase-Shift Keying (QPSK) and Quadrature Amplitude Modulation (QAM) formats at the RF output [11].

In the research, the AD8346EVAL modulation board was chosen as a complement the AD8347EVAL demodulator board. The functional block diagram of the AD8346EVAL broad is shown in Figure 18.

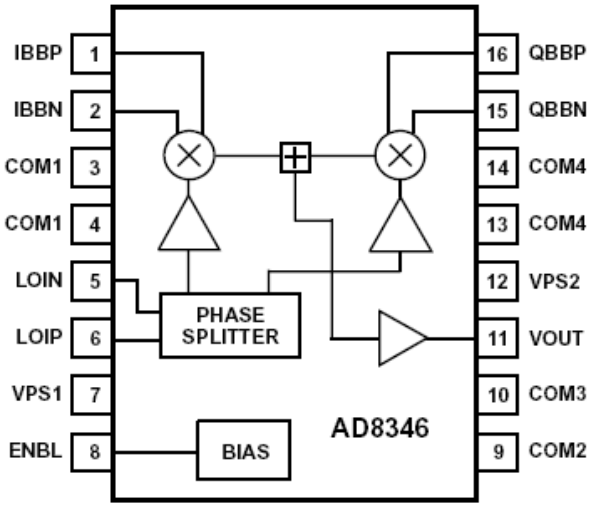

Figure 18. Functional block diagram of the AD8346EVAL quadrature modulator

B. WIRED LO DISTRIBUTION

1. Experimental Set-up

A wired setup for the distribution of the LO signal to two AD8346EVAL boards was first done to gather baseline results. The setup is as shown in Figure 19. In the setup, the LO signal was split using a power splitter and connected to the LO input of two AD8346EVAL boards. The LO inputs needed to be attenuated to ensure that the drive level was kept within the specifications of the AD8346EVAL board, i.e., between -6 to -12 dBm. In the experiment, a total of 39 dB of attenuation was connected at the output of the LO amplifier to give an optimum LO drive level of about -8 dBm. The RF outputs from the two AD8346EVAL boards were added via a power splitter before they were connected to a digital power meter for the readouts. LABVIEW control software was used to generate the phase of the RF output of the AD8346EVAL boards. The phase of one board was kept unchanged at 0 deg while the other was set from 0 to 350 deg at 5 deg increments.

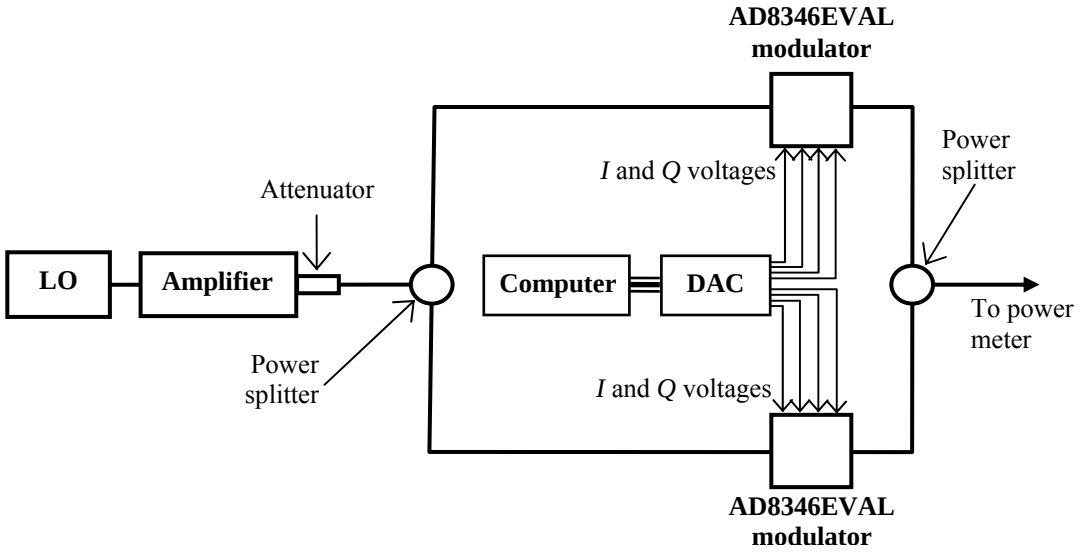

Figure 19. Experimental set-up for a wired LO distribution.

2. Results

The plot of the RF outputs from the two modulators, i.e., the sum of power received, is shown in Figure 20. The result shows a sinusoidal-square power curve with respect to the phase difference. Peak power is received at around 90 deg phase-difference and the minimum power is received at 270 deg phase-difference, which corresponds to a 180 deg spread. The peak-to-trough drop in power is about 16 dB. The result from the experiment demonstrates the constructive and destructive interference of the RF outputs from the two modulators across the various phase differences.

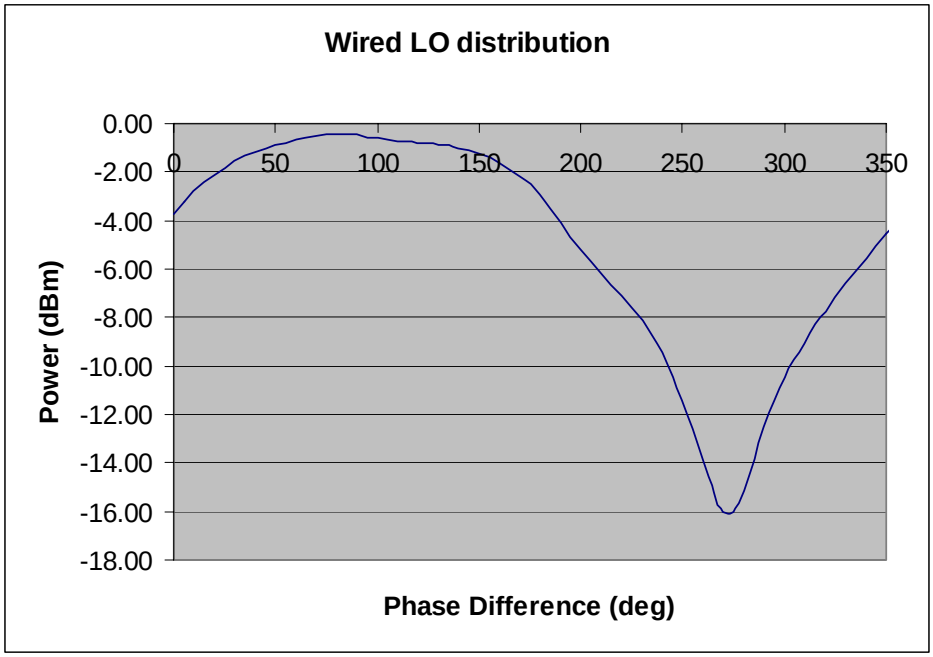

Figure 20. Array output for wired LO distribution

C. SIMULATION OF WIRELESS LO DISTRIBUTION

1. Multipaths Calculation

The results of the wireless LO distribution can be modeled using MATLAB. The set-up of the simulation is modeled after the experiment, with one source point (for the LO antenna) and two observation points (for two modulator antennas) contained within an absorbent lined box. Figure 21 shows the locations of these points and the multipath radiations from the source and reflections off the walls of the box.

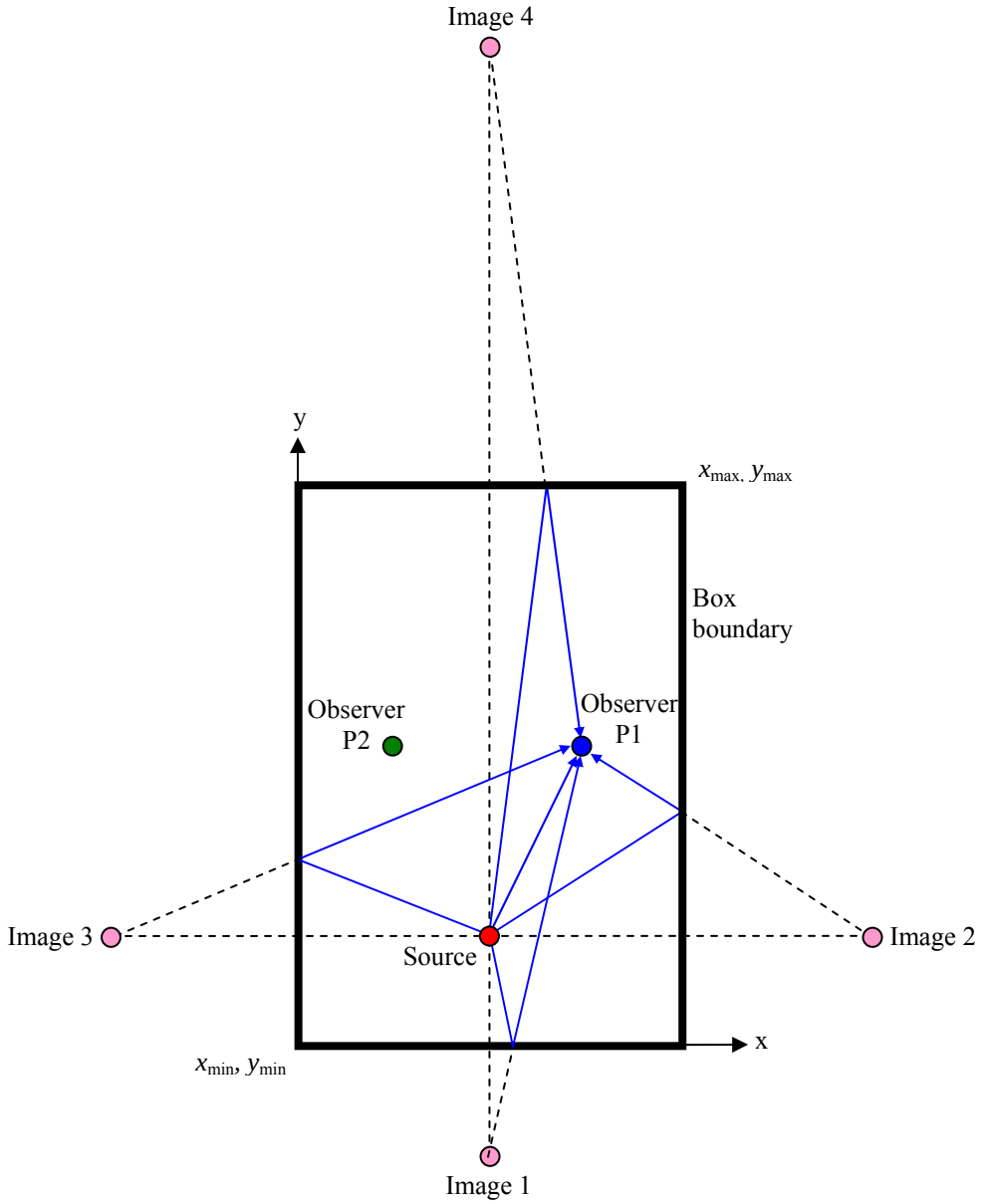

Figure 21. Setup of computer simulation for wireless LO distribution

Within the four-sided box, each observation point would receive signal direct from the source, and from four imaginary sources (Images 1 to 4) reflected off each of the four walls. The coordinates of these image sources are given by

$$x_{I1} = x_s \ , \qquad y_{I1} = y_{\min} - (y_s - y_{\min}) \tag{4.1}$$

$$x_{I2} = x_{\max} + (x_{\max} - x_s) \ , \quad y_{I2} = y_s \tag{4.2}$$

$$x_{I3} = x_s \ , \qquad y_{I3} = y_{\max} + (y_{\max} - y_s) \tag{4.3}$$

$$x_{I4} = x_{\min} - (x_s - x_{\min}) \ , \quad y_{I4} = y_s \tag{4.4}$$

where x_{I1}, y_{I1} = Coordinates of Image 1

x_{I2}, y_{I2} = Coordinates of Image 2

x_{I3}, y_{I3} = Coordinates of Image 3

x_{I4}, y_{I4} = Coordinates of Image 4

x_s, y_s = Coordinates of source point

$x_{\min}, y_{\min}$ = Reference coordinates of box

$x_{\max}, y_{\max}$ = Maximum coordinates of box

The electric fields received by the two observer points are summed to produce a plot similar to the array output of the two modulators. The electric field at the observer point from source and the reflections is then given by

$$E_{total} = \frac{e^{-jkR_{dir}}}{R_{dir}} + \sum_{n=1}^{4} e^{-jkR_n} \frac{\Gamma_n}{R_n} \tag{4.5}$$

where R_{dir} $= \sqrt{(x_p - x_s)^2 + (y_p - y_s)^2}$ is the direct distance from the source to observer point (x_p, y_p)

R_n $= \sqrt{(x_p - x_{In})^2 + (y_p - y_{In})^2}$ is the distance from Image n to observer at point (x_p, y_p)

x_p, y_p = Coordinates of observer point

Γ_n = Reflection coefficient of wall n

k $= \frac{2\pi}{\lambda}$ is the wave number

λ = Wavelength

The results of the computer simulation are discussed in the next section, where they are compared to the results of the physical experiment.

D. WIRELESS LO DEMONSTRATION

1. Experimental Set-up

The setup for the wireless LO distribution is as shown in Figure 22. It was similar to the wired setup except for the "stubby antennas" for the distribution of the LO signal, as well as the reception of the LO signal at the modulator boards. These "stubby antennas" were generic antenna specified for 2.4 GHz frequency. To reduce the effects of multipaths of the LO signals, the wireless setup was contained in a box made out of absorbent materials tuned to absorb the reflected signals. Pictures of the wireless setup are shown in Figure 23 and Figure 24.

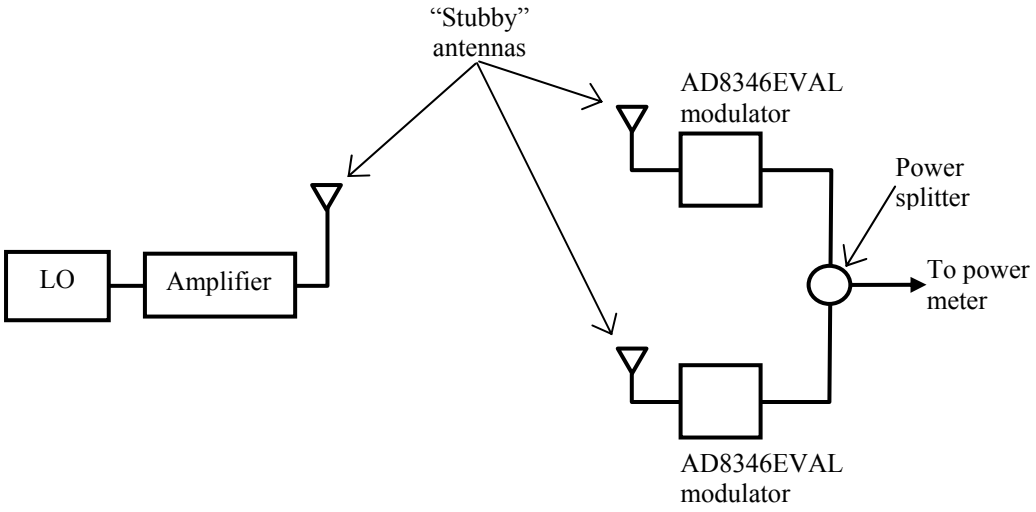

Figure 22. Experimental set-up for wireless LO distribution.

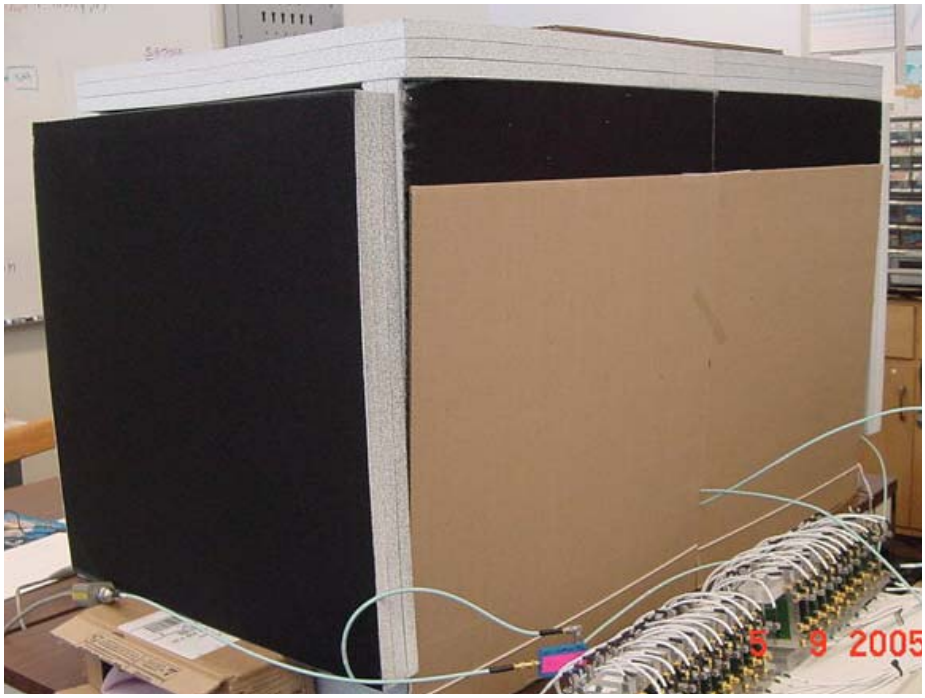

Figure 23. External view of the absorbent box for wireless LO demonstration.

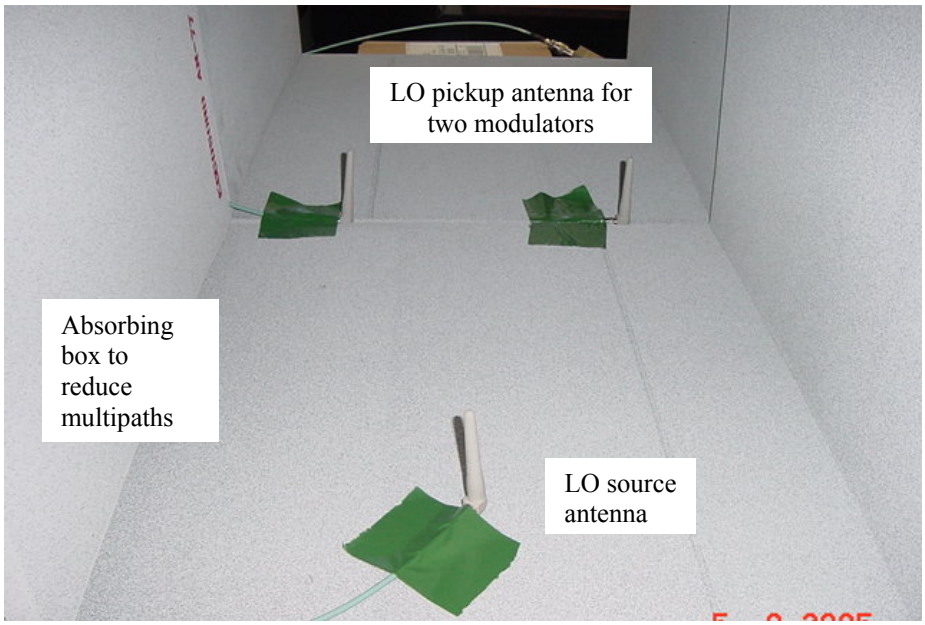

Figure 24. Setup of antennas in absorbing box for wireless LO demonstration.

2. Results

The array outputs from the two modulators at various phase differentials are tabulated in Table 2. This measured result is plotted against the expected results derived from the computer simulation in Figure 25.

Modulator 1 Amplitude (V)	Modulator 2 Amplitude (V)	Phase difference Modulator 1 and 2 (deg)	Array output (dBm)
5	5	0	-1.92
5	5	10	-2.05
5	5	20	-2.06
5	5	30	-2.25
5	5	40	-2.64
5	5	50	-2.98
5	5	60	-3.28
5	5	70	-3.78
5	5	80	-4.52
5	5	90	-5.57
5	5	100	-7.22
5	5	110	-8.4
5	5	120	-9.7
5	5	130	-11.04
5	5	140	-12.4
5	5	150	-14.1
5	5	160	-16
5	5	170	-18.76
5	5	180	-18.1
5	5	190	-14.45
5	5	200	-11.78
5	5	210	-10.23
5	5	220	-9.23
5	5	230	-8.05
5	5	240	-6.9
5	5	250	-5.7
5	5	260	-5
5	5	270	-4.3
5	5	280	-3.53
5	5	290	-3.07
5	5	300	-2.7
5	5	310	-2.49
5	5	320	-2.08
5	5	330	-2.03
5	5	340	-1.93
5	5	350	-1.91
5	5	360	-1.85

Table 2. Array outputs of modulators with wireless LO distribution.

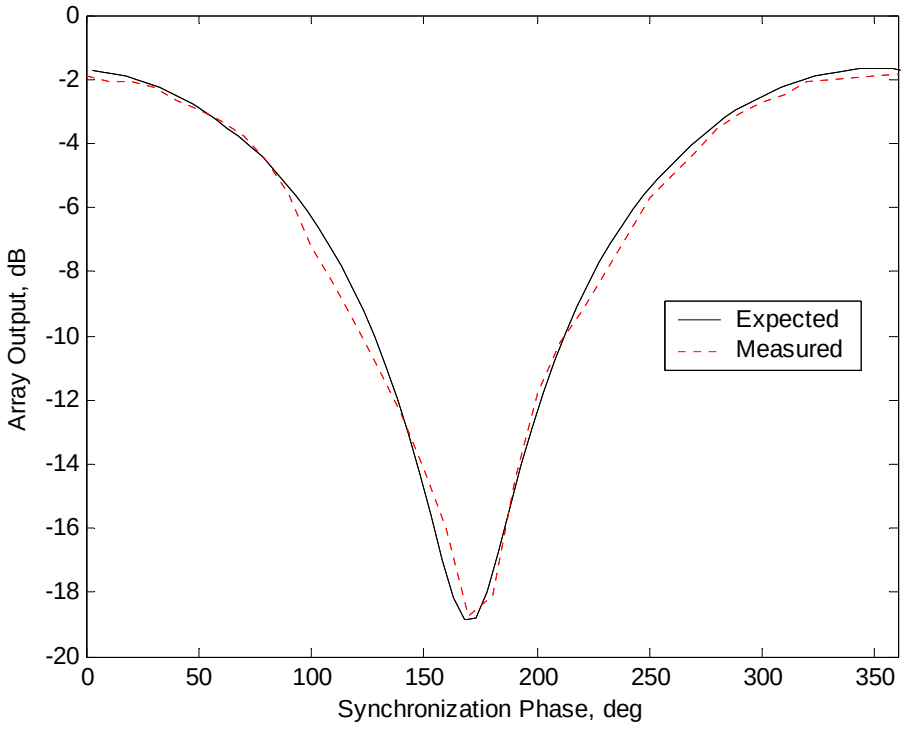

Figure 25. Expected and measured array outputs of modulators with wireless LO distribution.

The plots of the expected and measured results of the wireless LO are similar. Peak power is received at around 0/360 deg phase-difference and minimum power occurs at 180 deg phase-difference, which corresponds to a 180 deg spread. The peak-to-trough drop in power measured is about 16 dB, which is comparable to the wired set-up. The experiment successfully demonstrates the wireless distribution of the LO signals to the modulators in a controlled environment.

3. Further Investigation – Amplitude Variations

Further investigations were also conducted in the array output to see the effects of amplitude imbalance between the two modulators. The amplitude of one modulator input was set from 0 to 5 V at 0.25 V increment while the amplitude of the second modulator was kept constant at 5 V. This was repeated at a fixed 0 and 45 deg phase-difference between the two modulators. The objective was to substantiate the additive and subtractive interference of the two modulator outputs.

The expected results of the array output were modeled in MATLAB. Since the outputs of the two modulators are sinusoidal, the expected results from small increments of the amplitude of one modulator were also sinusoidal. The expected results were then plotted against the measured results for direct comparison. The results at 0 deg phase difference are tabulated in Table 3 and plotted in Figure 26, while the results at 45 deg phase difference are tabulated in Table 4 and plotted in Figure 27. The measured results are in general agreement with the computer simulation.

Modulator 1		**Modulator 2**		
Amplitude (V)	**Phase (deg)**	**Amplitude (V)**	**Phase (deg)**	**Array output (dBm)**
5	45	5	0	-2.12
5	45	4.75	0	-2.14
5	45	4.5	0	-2.18
5	45	4.25	0	-2.23
5	45	4	0	-2.29
5	45	3.75	0	-2.36
5	45	3.5	0	-2.45
5	45	3.25	0	-2.56
5	45	3	0	-2.69
5	45	2.75	0	-2.86
5	45	2.5	0	-3.05
5	45	2.25	0	-3.29
5	45	2	0	-3.57
5	45	1.75	0	-3.90
5	45	1.5	0	-4.26
5	45	1.25	0	-4.69
5	45	1	0	-5.16
5	45	0.75	0	-5.66
5	45	0.5	0	-6.18
5	45	0.25	0	-6.69
5	45	0	0	-7.19

Table 3. Amplitude variation of wireless LO at fixed 0 deg phase difference.

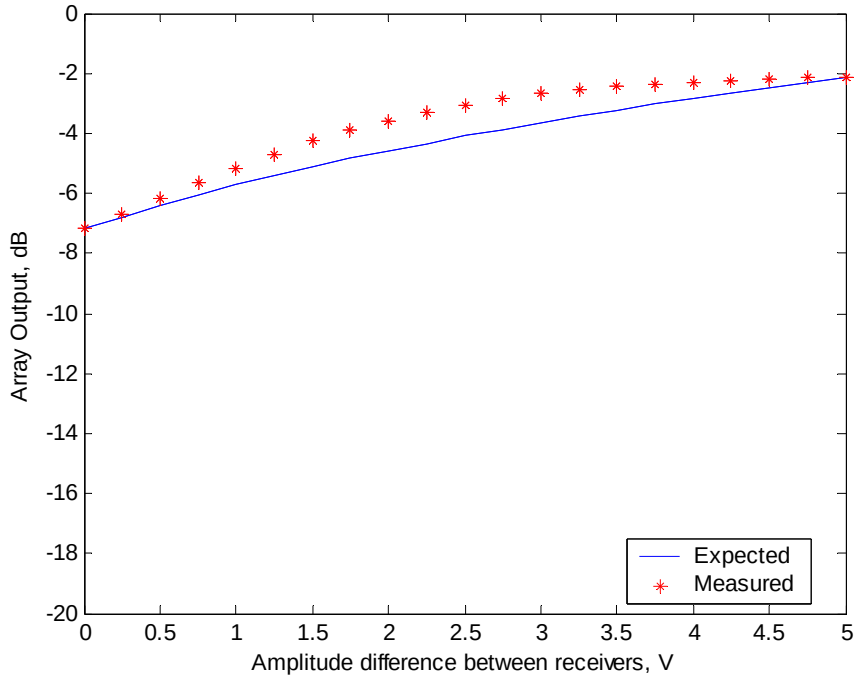

Figure 26. Amplitude variation in wireless LO distribution (0 deg phase difference).

Modulator 1		Modulator 2		
Amplitude (V)	**Phase (deg)**	**Amplitude (V)**	**Phase (deg)**	**Array Output (dBm)**
5	45	5	90	-5.63
5	45	4.75	90	-5.69
5	45	4.5	90	-5.78
5	45	4.25	90	-5.91
5	45	4	90	-6.06
5	45	3.75	90	-6.21
5	45	3.5	90	-6.40
5	45	3.25	90	-6.61
5	45	3	90	-6.86
5	45	2.75	90	-7.12
5	45	2.5	90	-7.38
5	45	2.25	90	-7.65
5	45	2	90	-7.90
5	45	1.75	90	-8.15
5	45	1.5	90	-8.37
5	45	1.25	90	-8.47
5	45	1	90	-8.45
5	45	0.75	90	-8.33
5	45	0.5	90	-8.09
5	45	0.25	90	-7.72
5	45	0	90	-7.19

Table 4. Amplitude variation of wireless LO at fixed 90 deg phase difference.

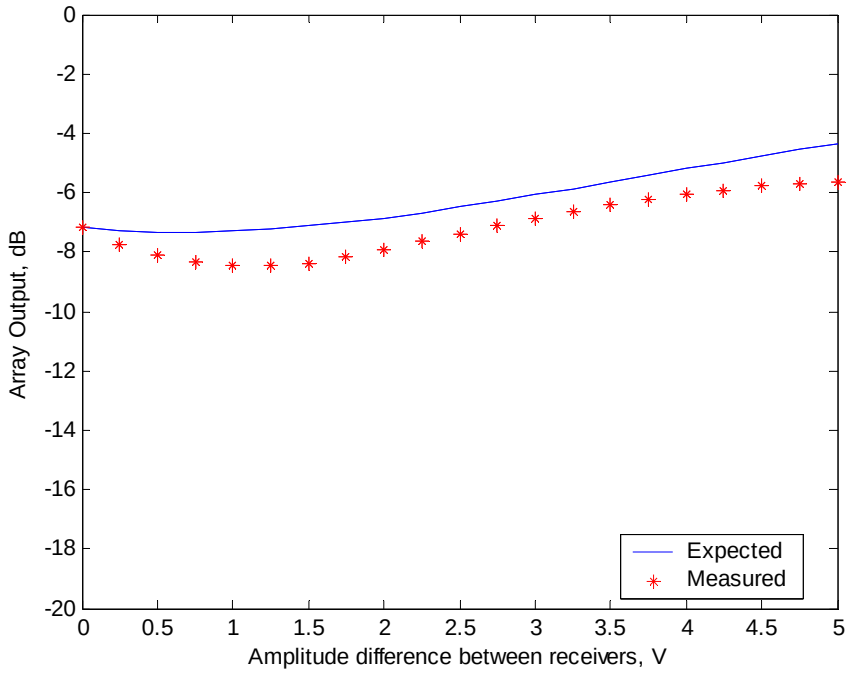

Figure 27. Amplitude variation in wireless LO distribution (45 deg phase difference).

E. SUMMARY

The chapter discussed the demonstration of a wireless LO distribution for a 2-element transmit array. An absorbent box was constructed to provide a "clean" environment such that the multipaths of the distribution could be accounted for. The experiment showed a good agreement in power received between a wired and wireless set-up, as well as between the expected and measured wireless set-up.

THIS PAGE INTENTIONALLY LEFT BLANK

V. DIGITIZATION AND SYNCHRONIZATION OF THE RECEIVE MODULES

In the bench test of the AD8347EVAL demodulation board, four digital multimeters were used to read the *I* and *Q* voltages off the board. Calculations of the phase angle from the *I* and *Q* readings were done separately. With the implementation of thousands of receive modules in the opportunistic array, it will be necessary to automate the calculations of these phase angles. This chapter covers the digitization of the receive *I* and *Q* voltages.

A. NATIONAL INSTRUMENTS PXI-5112 DIGITIZER

The National Instruments PXI-5112 is a PCI-based, low cost digital-to-analog converter (ADC). It features a high transfer rate over a large analog input range of ± 25 mV to ± 25 V. Each of the two analog input channels has its own 8-bit analog-to-digital converter for simultaneous data acquisition on each channel at rates up to 100 MSamples/s. With the NI5112 high-precision timing circuitry, the sampling rate of repetitive signals up to 2.5 GSamples/s is also possible.

A synchronization bus routes timing and trigger signals between two or more NI5112 modules. This allows multi-instrument synchronization by triggering several measurement devices with a signal from a single instrument and synchronizing all the instruments to the same clock. Control of the NI5112 digitizers is made implemented in LABVIEW, a GUI-driven control and simulation software package from National Instruments.

B. DIGITIZATION OF RECEIVE MODULE

The setup for the digitization of the receive module using the NI5112 digitizers is the same as that for the AD8347EVAL demodulator board bench test in Figure 13, except that the *I* and *Q* outputs of the demodulator board are now connected to the NI5112 digitizers. An external trigger was used for timing of the data sampling. Two NI5112 digitizer cards are required to read the four *I* and *Q*

outputs from one demodulator board. IOPP and QOPP are connected to Channel 0 and Channel 1 of the "Master" NI5112 card. IOPN and QOPN are connected to Channel 0 and Channel 1 of the second, "Slave" NI5112 card. This pairing facilitates the calculation of *I(t)* = IOPP – IOPN and *Q(t)* = QOPP – QOPN for the determination of the phase angle in Equation (2.9). The experimental set-up is shown in Figure 28, and the connections on the digitizers are shown in Figure 29.

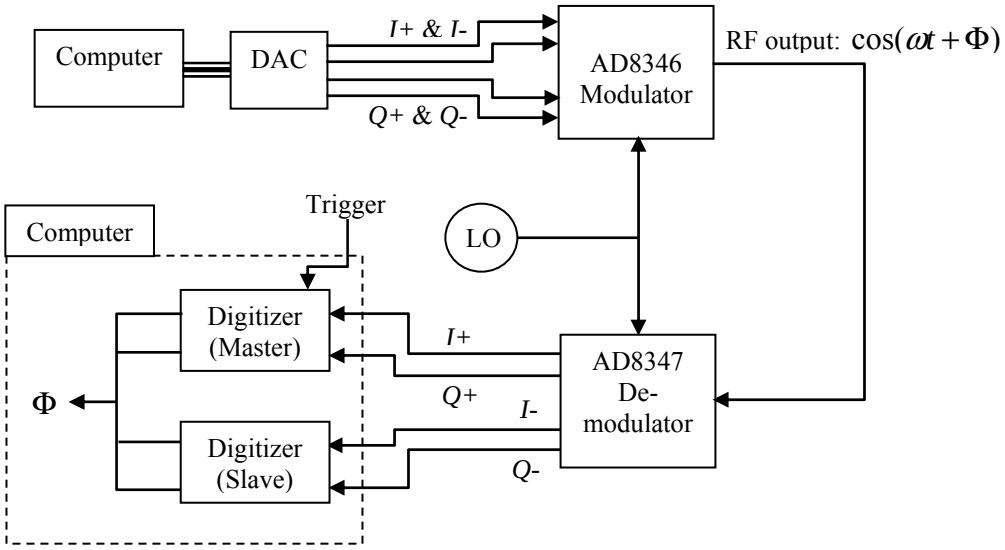

Figure 28. Digitization of *I* and *Q* voltages.

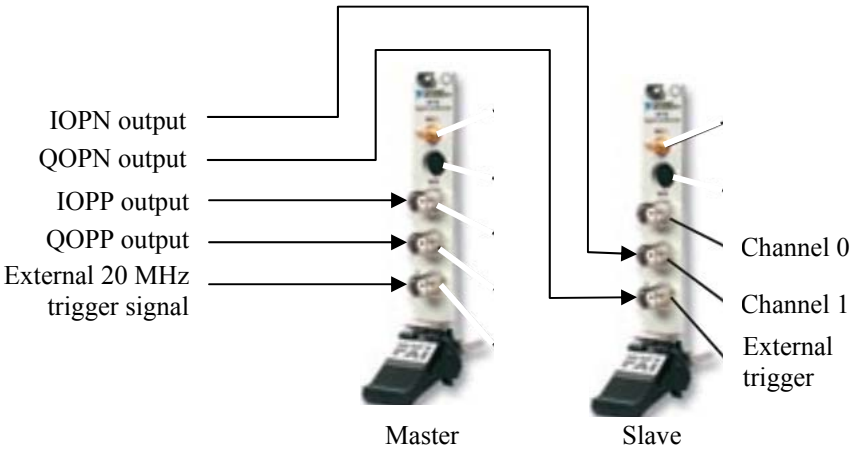

Figure 29. NI5112 digitizer connections.

A LABVIEW program from the software library was customized for the conversion of the *I* and *Q* voltages into quadrature phase angle based on Equation (2.9). The front panel of the program is shown in Figure 30. The VGIN input for the AD8347EVAL demodulator board was lowered to 0.25 V in order that there was sufficient gain in the demodulation for the operation of the digitizers.

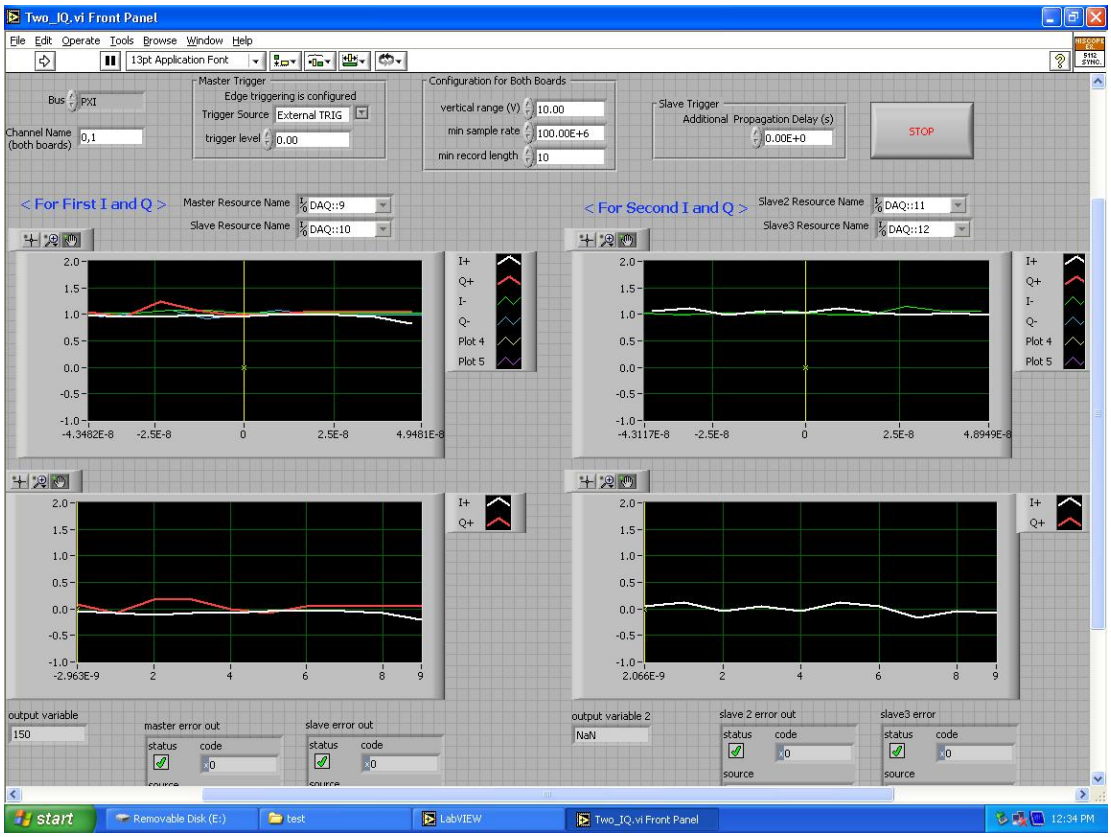

Figure 30. Customised LABVIEW software for digitization of receive modules.

C. RESULTS AND ANALYSIS

Table 5 tabulates the readings taken off the LABVIEW program as the transmit signal phase was shifted from 0 to 330 deg. An AD8346EVAL board was used to provide the phase-shifted transmitted signal. The results are plotted in Figure 31.

Phase input at transmit module (deg)	Phase output at receive module (deg)
0	-94
30	-92
45	-69
60	-45
90	0
120	49
135	49
150	49
180	91
210	94
225	107
240	133
270	133
300	180
315	-135 (225)
330	-137 (227)

Table 5. Phase inputs at modulator and outputs at demodulator.

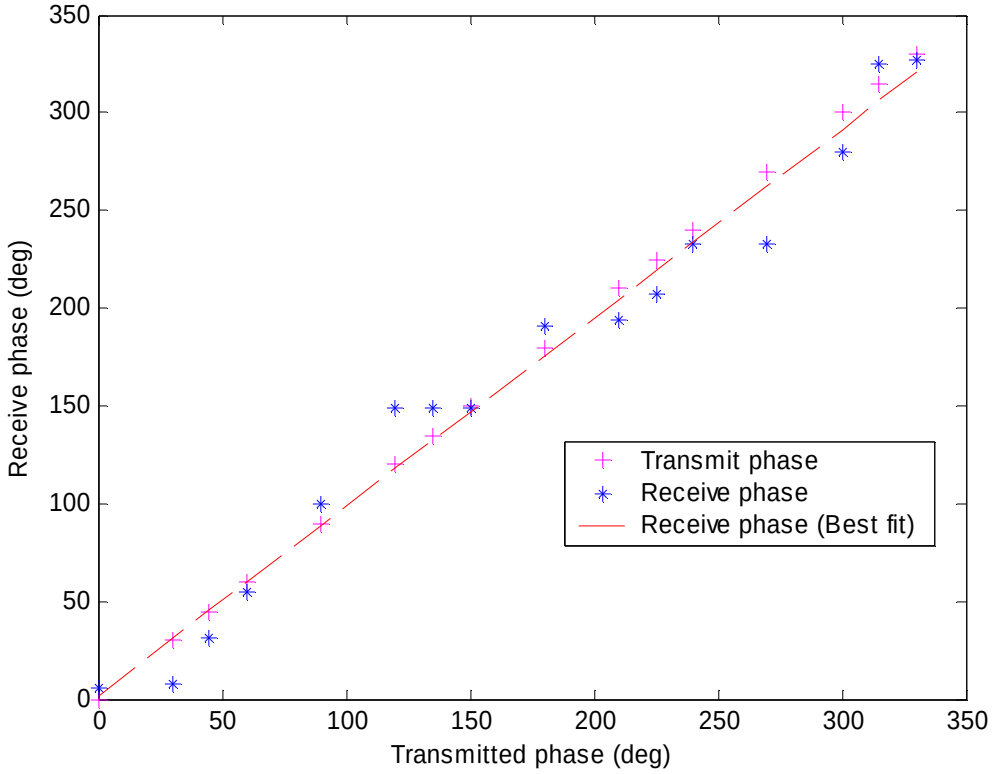

Figure 31. Transmit phase versus receive phase.

Ideally, the receive and transmit phases should be identical, except for a constant, i.e., the plot should be a straight line. There is a linear relationship between the two. For example, when the transmit signal is shifted 90 deg, the demodulator board should detect a 90 deg phase shift. As seen in Figure 31, the measured results were in general agreement with the transmit phase, but not as good as the results of the AD8347EVAL demodulator board bench test in Chapter III. This is attributed to the following factors.

1. Incorrect Gain Control in the Demodulator

In [3], the demodulator was set to automatic gain control where output voltages (VGA) from the onboard detectors were used as the gain control input (VGIN) for the demodulator. This resulted in a rippled response between the transmit and receive phase, as shown in Figure 32.

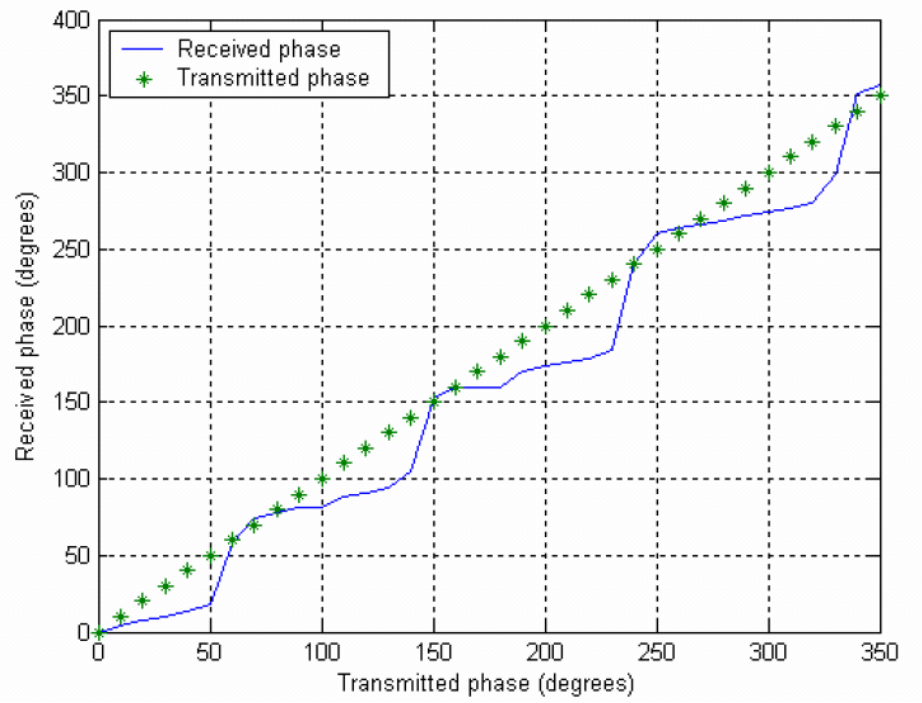

Figure 32. Previously measured response between transmit and receive phase with AGC mode turned 'on' (From [3]).

This error was subsequently corrected in [4] when a fixed gain input of 0.7 V was provided at VGIN. According to [12], a VGIN range of 0.5 to 0.9 V would give zero gain error and zero linearity error in the demodulator, as shown in Figure 33. However, the gain and linearity error would increase to -10 dB and -4 dB respectively

when VGIN is set at 0.25 V. In the digitized demodulator setup, it was necessary to increase the gain of the demodulator to almost 39.5 dB with VGIN set at 0.25 V. This was necessary so that there is adequate signal level for the operation of the NI5112 digitizers. However, at this gain the linearity error is significant, as shown in Figure 33. This is one reason behind the poor agreement of the receive and transmit phase in Figure 31. To circumvent this problem of saturation, an operational amplifier could be used to boost the signal outputs of the demodulator board to a level that would ensure the proper operation of the NI5112 digitizers.

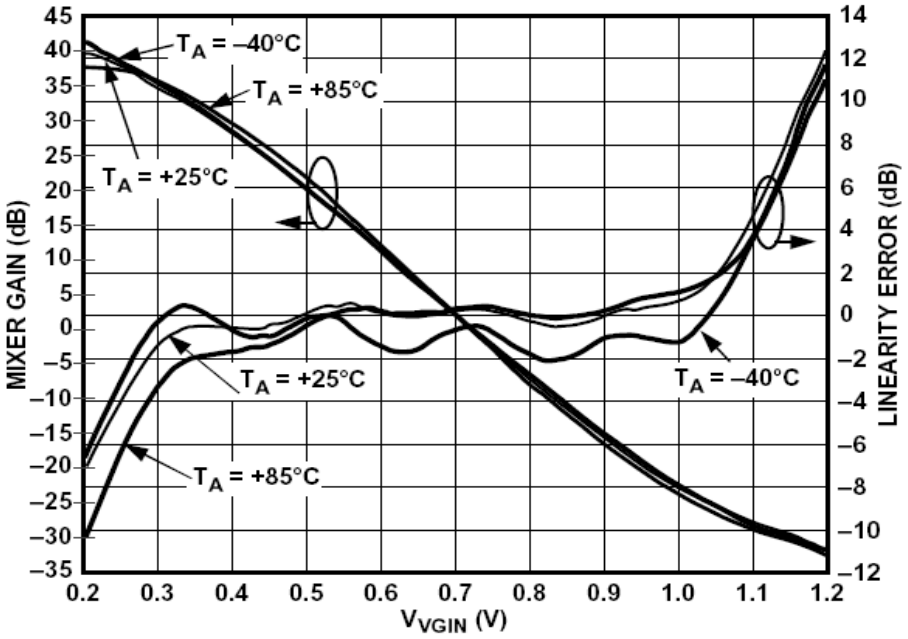

Figure 33. Gain and linearity error of AD8347EVAL demodulator board (From [12]).

2. Quantization Error of the NI5112 Digitizer

From the AD8347EVAL demodulator board bench test in Table 1, for a VGIN range of 0.5 to 0.9 V, a resolution of 1 mV was necessary for the readouts of the *I* and *Q* voltages for 10 deg increments in the transmit phases. In the digitization of the demodulator board, the voltage range of the measured *I* and *Q* outputs, with VGIN set at 0.25 V, was -1.0 to 3.0 V. The NI5112 digitizer was specified at 8 bit resolution, which only gives a 15.6 mV resolution for the *I* and *Q* readouts. Therefore, the 8-bit NI5112 digitizer does not have the resolution to read a 1 mV change in

voltage. To improve the resolution, either a 16-bit digitizer, which would give 0.06 mV resolution for a 4 V readout range, or an operational amplifier with gain would be necessary.

D. SYNCHRONIZATION OF THE RECEIVE MODULES

Following the digitization of the receive module, the synchronization of a two element receive array was investigated. Two demodulators were used to simulate a two-element array. A mechanically adjustable phase shifter was used at one of the two demodulators, while the other demodulator was used as reference. The set-up is shown in Figure 34 and the connections for the demodulator boards are shown in Figure 35. By manually adjusting the phase shifter, a corresponding phase output from the demodulator can be observed. This demonstrated the successful synchronization of the demodulation, which is a necessary step in developing a high performance receive array.

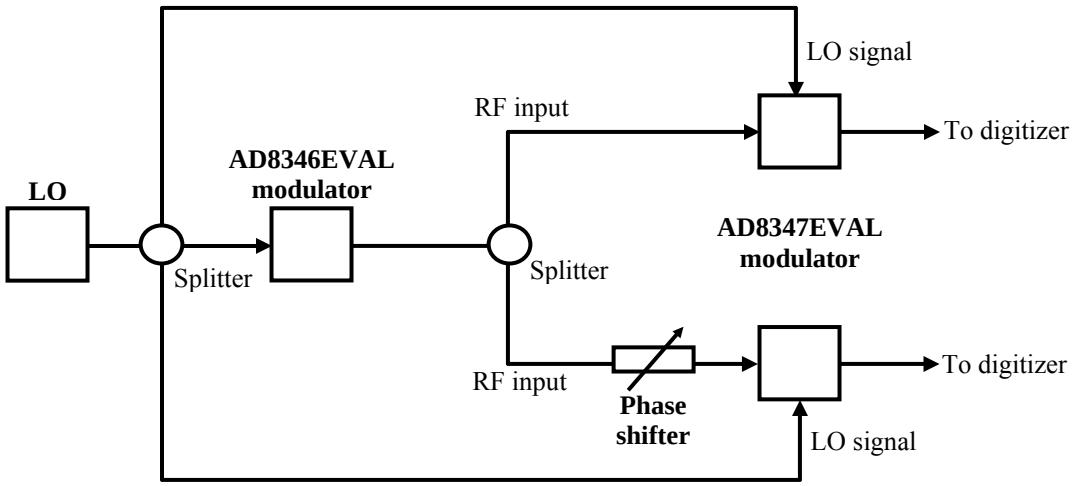

Figure 34. Synchronization of two receive modules.

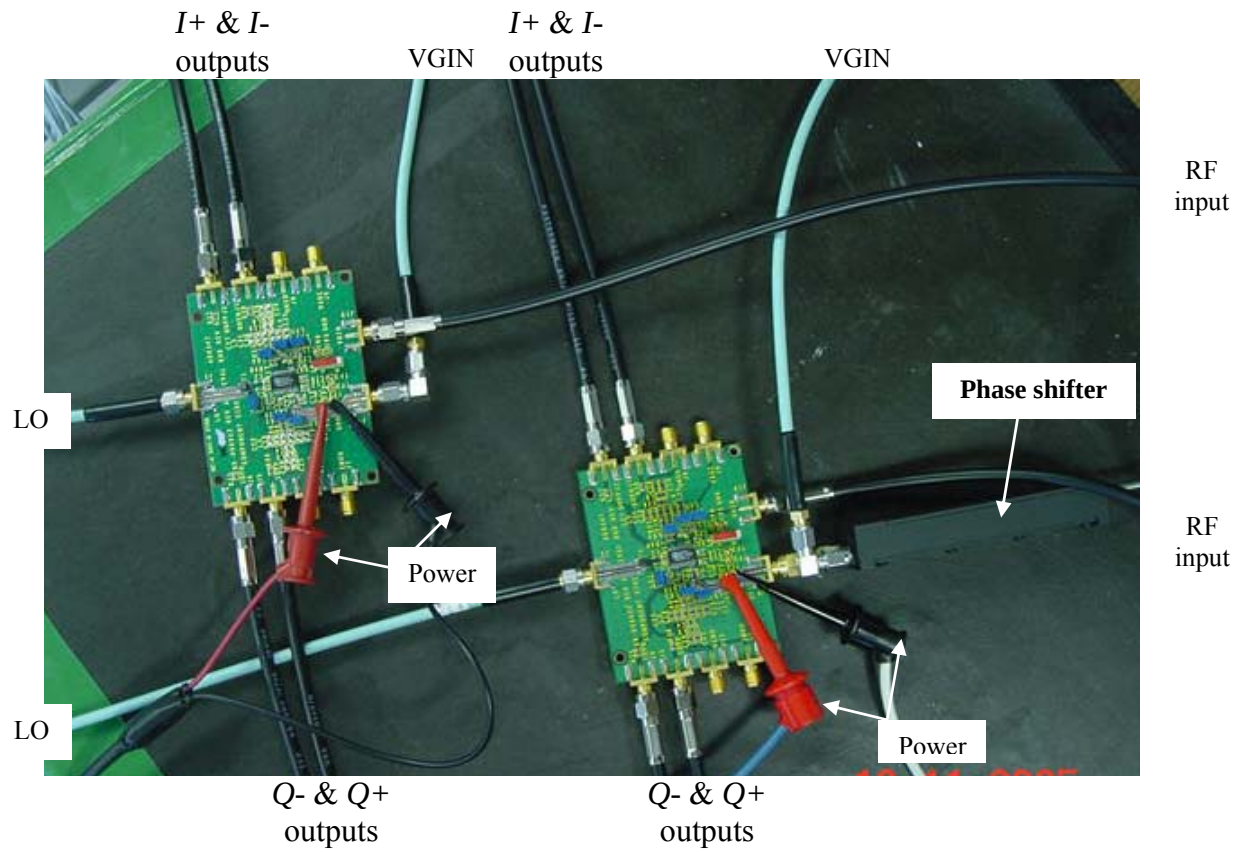

Figure 35. Connections of two AD8347EAVL demodulator boards.

E. SUMMARY

This chapter discussed the digitization of the receive modules. Using the NI5112 digitizers and a customized LABVIEW program for the measurement of the in-phase and quadrature outputs of the receive modules, the setup for the digitization of the receive module was successfully conducted. The experiment demonstrated a broadly linear response between the transmit and receive phase, which was limited by the resolution of the NI5112 digitizers. With an operational amplifier to boost the *I* and *Q* signal levels, better resolution and hence lower phase error could be achieved.

VI. TRANSMISSION SYSTEM

A. TRANSMISSION SYSTEM

In the proposed opportunistic array onboard the surface warship, the digital beamformer and controller are separate from the transmit and receive modules, as shown in Figure 7. As a result, the synchronizing LO signal and beam control data need to be sent wirelessly to the transmit modules, while the digitized radar signals from the receive modules would be sent in reverse to the digital signal processor for processing. The characteristics of the transmission medium within the ship's confines needs to be investigated to ensure minimal loss and proper propagation of these signals. It would be desirable if such a transmission medium would cater to all microwave and RF wireless systems onboard ship, for example, damage assessment sensors. Figure 36 shows a generic implementation of the integrated transmission system.

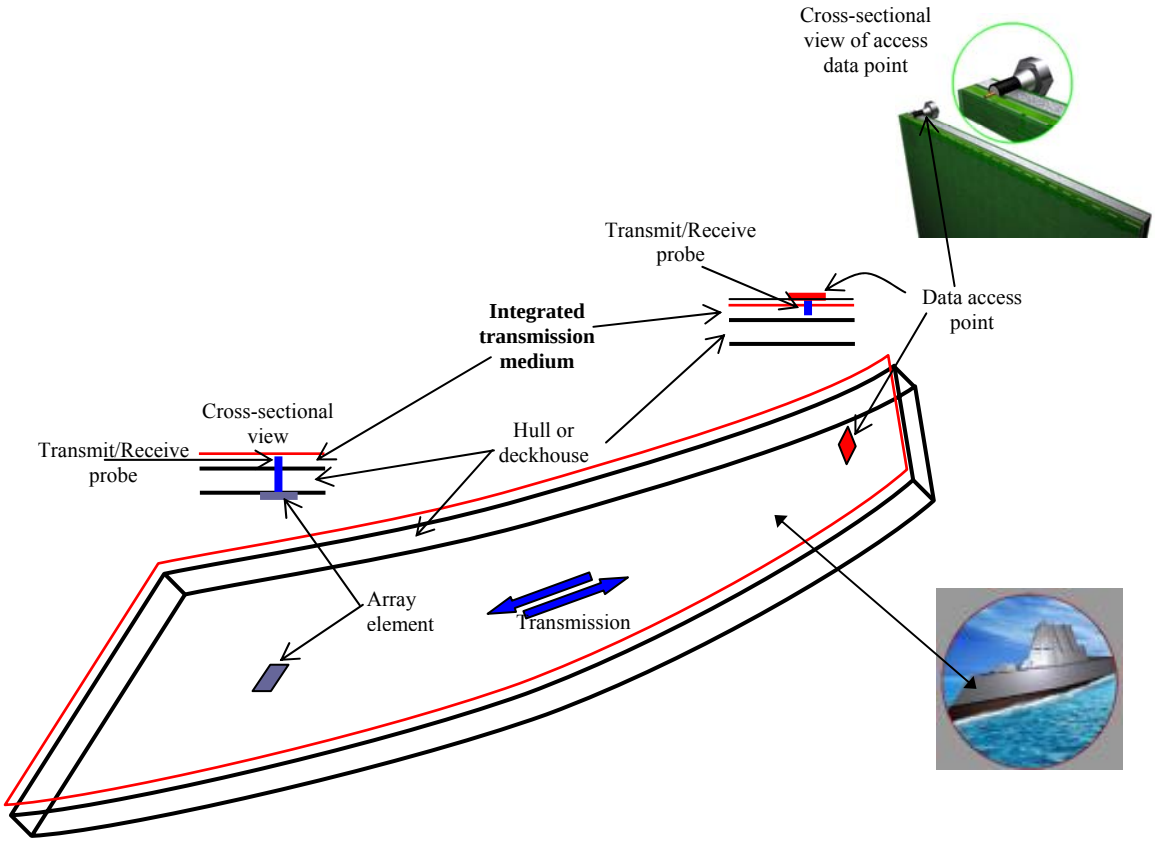

Figure 36. Integrated ship transmission system (After [11] and [14]).

The ideal transmission system would have the following features: low noise, low loss, wideband, simple to implement, easily integrated into the ship's hull or superstructure, scalable and low-cost. One candidate for the transmission system is a parallel-plate waveguide sandwiching a dielectric medium. Another candidate is a single-plate conducting plane with a thin film of dielectric, as shown in Figure 37. Both transmission system candidates will be discussed in this chapter.

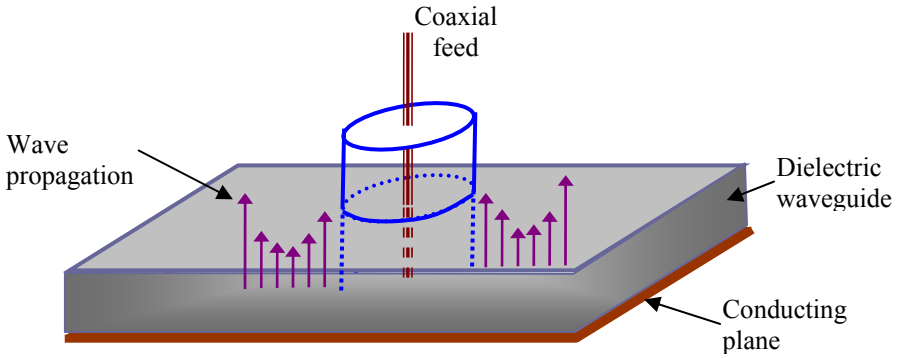

Figure 37. Propagation in a single-plate dielectric waveguide.

B. PARALLEL-PLATE TRANSMISSION SYSTEM

1. Transmission Loss Calculations

Since the implementation of the wireless transmission system in warships is inside its deckhouse and hull structures, the transmission can be modeled after a parallel-plate transmission line. Parallel-plate transmission supports transverse electromagnetic (TEM) waves at all frequencies. TEM waves are waves in which the electric (E) and magnetic (H) field are perpendicular to each other, and both are transverse to the direction of propagation along the guiding line. A plane wave is an example of a TEM wave.

Attenuation in a waveguide arises from two sources: lossy dielectric and imperfectly-conducting walls. These losses are expressed in the attenuation constant of the waveguide as a summation of the two losses.

$$\alpha = \alpha_d + \alpha_c \tag{6.1}$$

where α = attenuation constant

α_d = attenuation constant due to dielectric

α_c = attenuation constant due to ohmic losses in the imperfectly-conducting walls.

Thus, the fields of a TEM wave traveling a distance *d* in the medium between the plates will decrease in amplitude by a factor of $e^{-\alpha d}$. For TEM modes in parallel-plates, the attenuation constants have been derived in closed form [16]. For the dielectric losses,

$$\alpha_d = \frac{\sigma}{2}\sqrt{\frac{\mu}{\varepsilon}} = \frac{\sigma}{2}\eta \tag{6.2}$$

where ε = permittivity of dielectric medium = $\varepsilon_r\varepsilon_o$ ($\varepsilon_o = 8.85\times10^{-12}$ F/m)

μ = permeability of dielectric medium = $\mu_r\mu_o$ ($\mu_o = \frac{1}{4\pi}\times10^{-9}$ H/m)

σ = conductivity of dielectric medium , S/m

η = intrinsic impedance of dielectric = $\sqrt{\frac{\mu}{\varepsilon}}$, Ω

Note that for a lossless dielectric, $\sigma = 0$. Therefore, for the dielectric losses, $\alpha_d = 0$. As for the ohmic losses,

$$\alpha_c = \frac{1}{b}\sqrt{\frac{\pi f \varepsilon}{\sigma_c}} \tag{6.3}$$

where σ_c = conductivity of the metal plates

f = frequency

b = thickness of the dielectric, i.e., spacing between the plates

Loss tangent is a measure of the power loss in the medium and is derived from the complex form of the dielectric permittivity $\varepsilon = \varepsilon' - j\varepsilon'' = \varepsilon' - j\frac{\sigma}{\omega}$. Loss tangent is defined as

$$\tan\delta = \frac{\varepsilon''}{\varepsilon'} = \frac{\sigma}{\omega\varepsilon'} = \frac{\sigma}{\omega\varepsilon_o\varepsilon_r} \tag{6.4}$$

where ε_r = relative permittivity of dielectric

ω = $2\pi f$

Based on the above formulas, the power loss (dB per unit length) of a dielectric can be calculated. The dielectric chosen was the common Teflon material with a dielectric constant of 2.0 with a loss tangent of 0.004. The results are plotted in Figure 38. The power loss per unit length of the dielectric for different plate spacings, at 0.3 GHz, is tabulated in Table 6, which shows negligible power loss for all the three plate spacings.

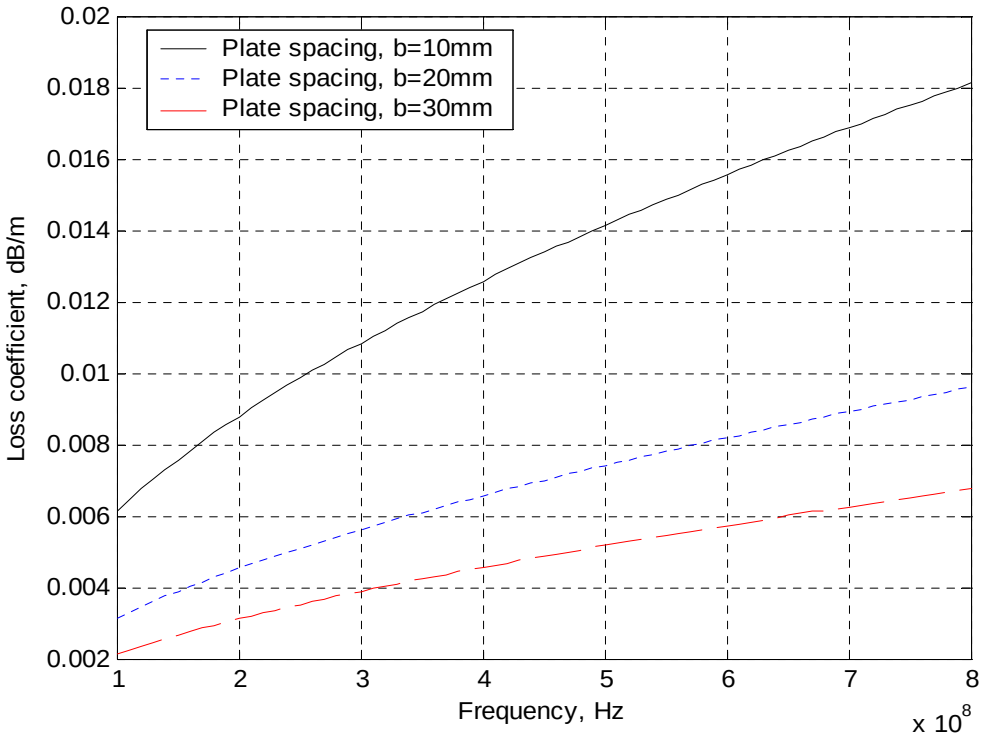

Figure 38. Transmission loss for parallel-plate dielectric with dielectric constant 2.0.

Plate spacing, b (mm)	Loss per unit length in dielectric (dB/m)
10	10.8×10^{-3}
20	5.6×10^{-3}
30	3.9×10^{-3}

Table 6. Power loss per unit length in dielectric.

2. Cylindrical (Two-Dimensional) Propagation

In a parallel-plate waveguide, the wave fields are contained in the dielectric medium within the parallel plates, as shown in Figure 39. If a probe is used to excite a field between the plates, the power spreads over a cylindrical wavefront. The power density at distance ρ from the source is thus given by

$$\frac{P}{2\pi\rho d} = \frac{E^2}{\eta} \tag{6.5}$$

where P = Power of source (W)

ρ = Radial distance from source (m)

d = Thickness of dielectric waveguide within parallel plates (m)

E = Electric field intensity (V/m)

η = Medium impedance (η = 377 Ω for free space)

From Equation (6.5), the spreading of the wave in the parallel plates can be derived, which shows the electric field proportional to the square-root of the distance from the source. Thus the field of a cylindrical wave has the form

$$E \sim \frac{1}{\sqrt{2\pi\rho}} e^{-jk\rho} \tag{6.6}$$

where k = $\frac{2\pi}{\lambda}$ is the wave number

$e^{-jk\rho}$ = Phase delay of the propagation at distance ρ

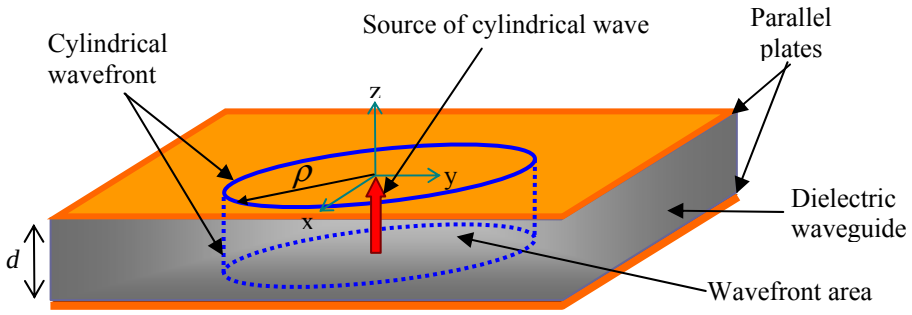

Figure 39. Cylindrical wavefront in parallel-plate transmission.

Microwave Studio was used to verify the cylindrical wavefunction of the parallal-plate waveguide. The two-dimensional phase plot is shown in Figure 40. It represents a "time snapshot" showing the expected cylindrical wavefronts. There is some small reflection from the edges of the parallel plates, which slightly distorts the wavefronts farthest from the source.

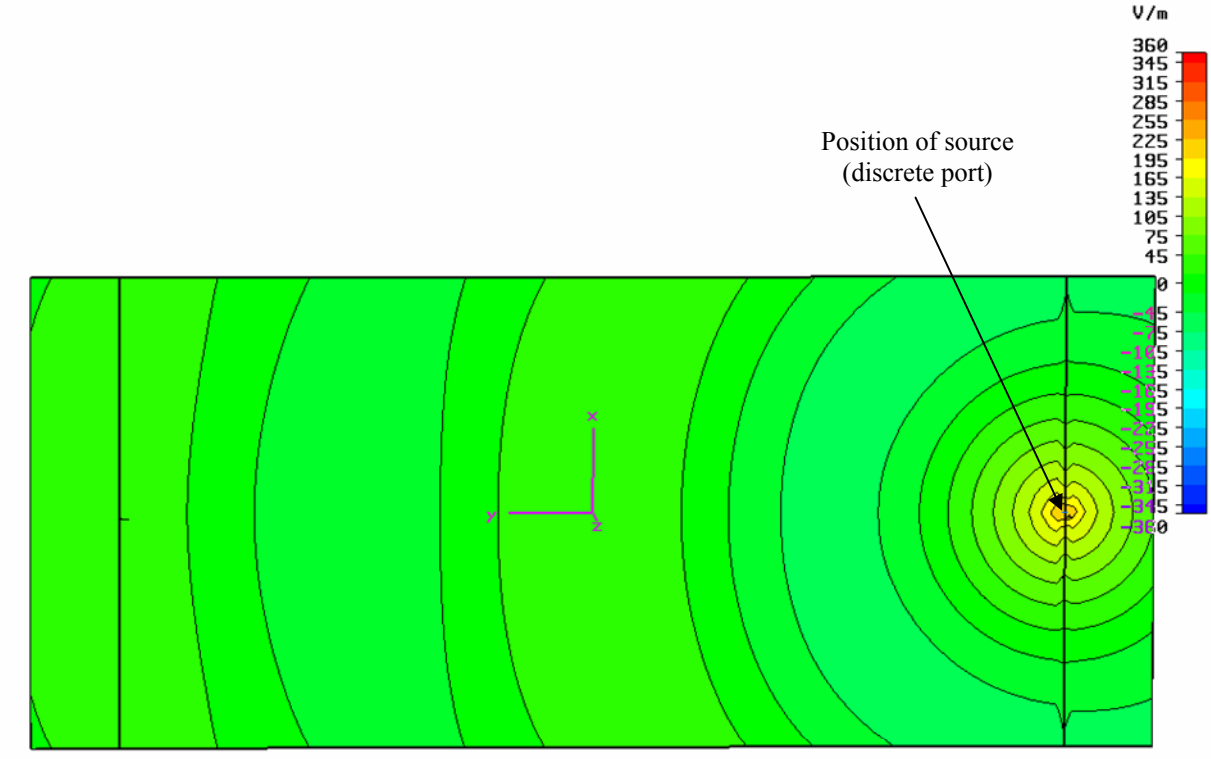

Figure 40. Phase plot of cylindrical wavefronts in parallel-plate waveguide.

3. Cylindrical and Spherical Propagation

From Equation (6.5), the power spreading for a two-dimensional cylindrical wave can be derived as

$$\frac{|E_{2D}|^2}{\eta} = \frac{P_t G_t}{2\pi\rho} \rightarrow E_{2D} = \frac{\sqrt{60 P_t G_t}}{\sqrt{\rho}} \tag{6.7}$$

where P_t = Transmitted power

G_t = Gain of the transmission probe (=1 for isotropic)

η = Medium impedance (η = 377 Ω for free space)

Similarly, the power spread for three-dimensional spherical wave propagation can also be derived as

$$\frac{|E_{3D}|^2}{\eta} = \frac{P_t G_t}{4\pi R^2} \rightarrow E_{3D} = \frac{\sqrt{30 P_t G_t}}{R} \tag{6.8}$$

where G_t = Gain of the antenna (=1 for isotropic), and R= Radial (spherical) distance from the source. Combining Equations (6.7) and (6.8) yields the ratio of two-dimensional to three-dimensional power spreading

$$\frac{P_{2D}}{P_{3D}} = \frac{(E_{2D})^2}{(E_{3D})^2} = \left(\frac{\sqrt{\frac{60 P_t G_t}{\rho}}}{\frac{\sqrt{30 P_t G_t}}{R}} \right)^2 \propto \frac{R^2}{\rho} \tag{6.9}$$

Equation (6.9) provides the relationship between the relative power received using two- and three-dimensional transmission systems. For a given minimum received power, waves can travel much farther in the two-dimensional medium versus the three-dimensional medium. This facilitates a direct comparison between the two as the preferred transmission system.

Since the beam controller is inside the ship and the array elements on its surface, the shortest path between the two will be direct line of sight, LOS (assuming no obstruction). The path around the perimeter of the ship, where the parallel plate transmission line is applied, is generally longer than the LOS. This is depicted in

Figure 41 for a rectangular shaped compartment. It is comprised of a point source at origin and an observation point moving along the three edges (legs) of a boundary box. The three-dimensional propagation is determined by the direct LOS distance R from the source to the observer, while the two-dimensional propagation is determined by the perimeter distance, ρ, traveled along the boundary box. MATLAB was used to investigate which of the two transmission media would incur less spreading loss.

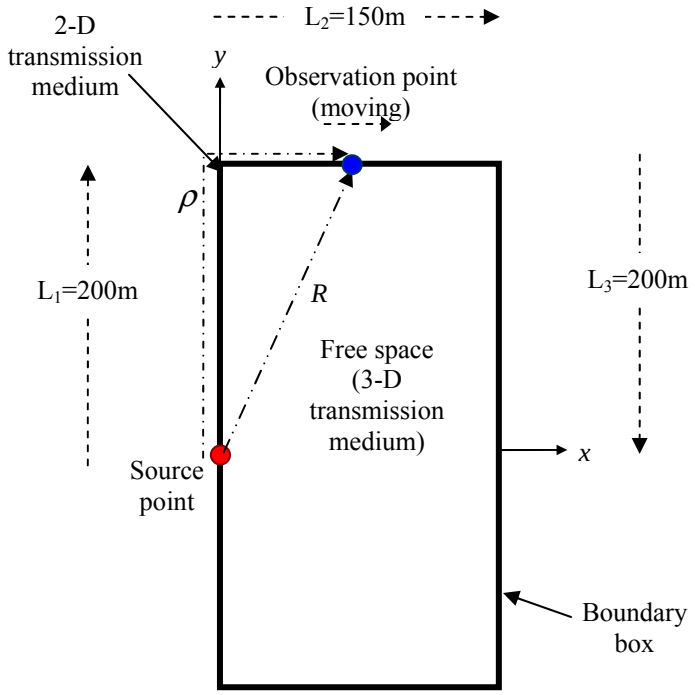

Figure 41. MATLAB model for the two- and three-dimension propagation.

The power ratio in Equation (6.9) is plotted, and is shown in Figure 42 for L_1=L_3=200 m and L_2=150 m. The plots show a power advantage for the cylindrical two-dimensional propagation over the spherical three-dimensional propagation. It should be noted that the computer simulation did not take into account the attenuation loss in the parallel plates.

From the results, the two-dimensional transmission medium has an advantage over the three-dimensional medium. The two-dimensional transmission medium is also more resistant to interference and does not generate EM emissions that can interfere with other systems. For ships, there is unlikely to be direct LOS path for the

transmission so the $\frac{1}{R^2}$ spreading is overly optimistic. The three-dimensional transmission will also need to overcome multipath and time-varying channel conditions.

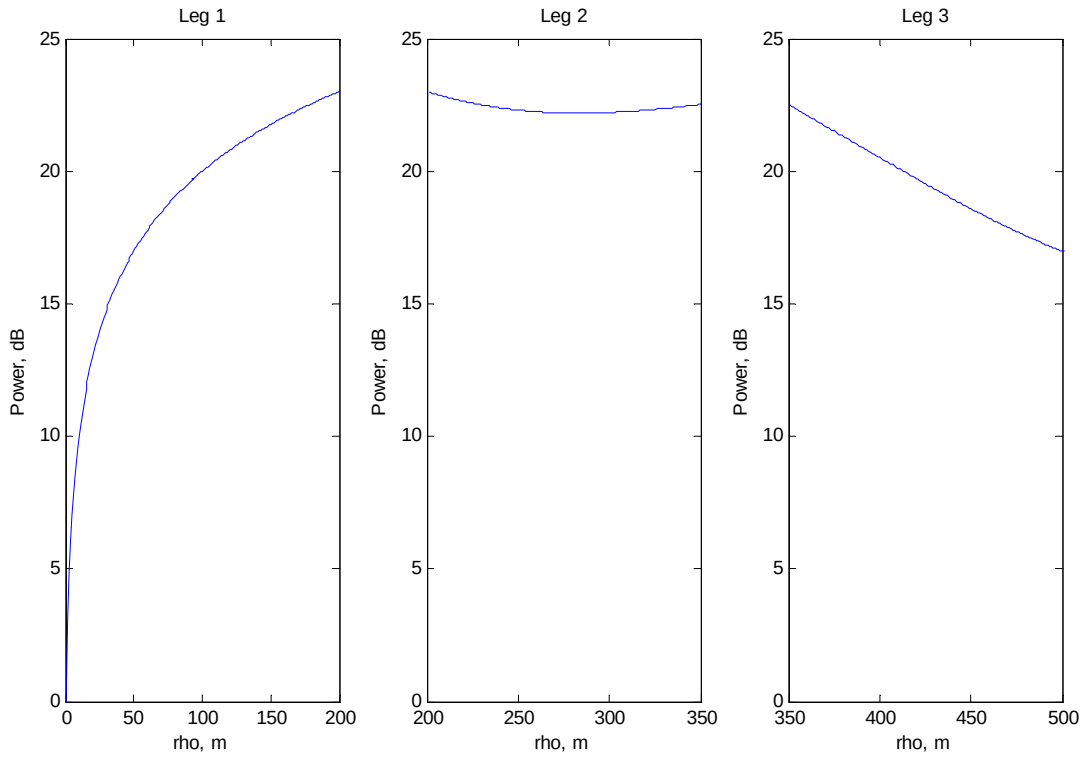

Figure 42. Power dissipation of two- and three-dimension propagation.

C. SINGLE-PLATE TRANSMISSION SYSTEM

1. Analysis of Conducting Plane with Thin Dielectric Coating

Reference [16] discusses the propagation of a TM surface wave along a conducting plane coated with a thin layer of dielectric. The results of the analysis showed that the thin film of dielectric can give rise to a large increase in the field concentration near the surface of the dielectric. With the proper choice of the dielectric constant and thickness, the attenuation constant of such a surface waveguide can be considerably less than that of a conventional rectangular waveguide. This makes the single-plate transmission system a possible candidate for the aperstructure.

The construct of the conducting plane coated with a thin-film dielectric is shown in Figure 43. The dielectric coating is of thickness t and has a complex dielectric constant $\varepsilon_r = \varepsilon'_r - j\varepsilon''_r$.

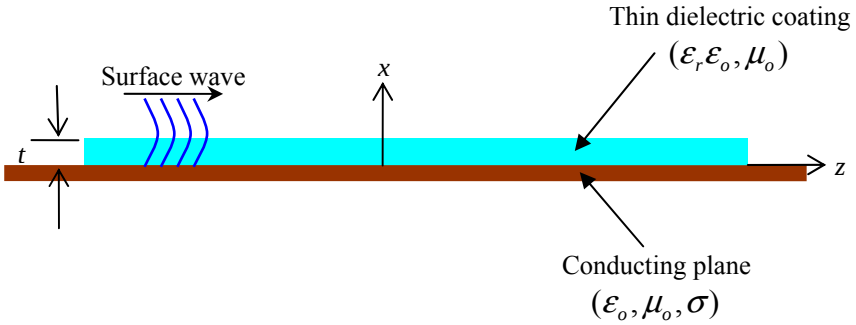

Figure 43. Conducting plane coated with thin layer of dielectric (After [14]).

From the impedances of the wave in free space and in the dielectric, the normalized surface impedance of the conductor can be derived as

$$Z_s = R_s + jX_s = (1+j)\left(\frac{k_o}{2\sigma Z_o}\right)^{1/2} \tag{6.10}$$

Where σ = conductivity of the conducting plane

k_o = $\frac{2\pi}{\lambda_o}$ is the free space wave number with wavelength λ_o

Z_o = 377 Ω is the impedance of free space

For a thin dielectric $(t << \lambda_o)$, only the dominant TM mode propagates along the surface. For this mode

$$H_y = \begin{cases} A\exp(jh_1 x - j\beta z), & x > t \\ [B\exp(jh_2 x) + C\exp(-jh_2 x)]\exp(-j\beta z), & 0 \le x \le t \end{cases} \tag{6.11}$$

From the equivalent circuit for propagation in the x direction, the traverse wave number h_1 can be derived and simplified as [14]

$$h_1 = k_o\left(Z_s + jk_o t\frac{\varepsilon_r - 1}{\varepsilon_r}\right) \tag{6.12}$$

The propagation constant β can also be calculated from

$$\beta = \left(k_o^2 - h_1^2\right)^{1/2} \tag{6.13}$$

2. Losses for Different Thickness and Dielectric Constant of the Dielectric Coating

MATLAB was used to plot the power loss at three wavelengths from the dielectric to show the field concentration near the surface, as well as the power loss per meter along the propagation direction z. The frequency for the simulation was set at 300 MHz. The simulation was repeated for dielectric constants 2.56, 10 and 20, as well as for thickness of the dielectric coating ranging from 0 to 10 mm. The MATLAB code is in the Appendix. The results obtained are shown in Figure 44.

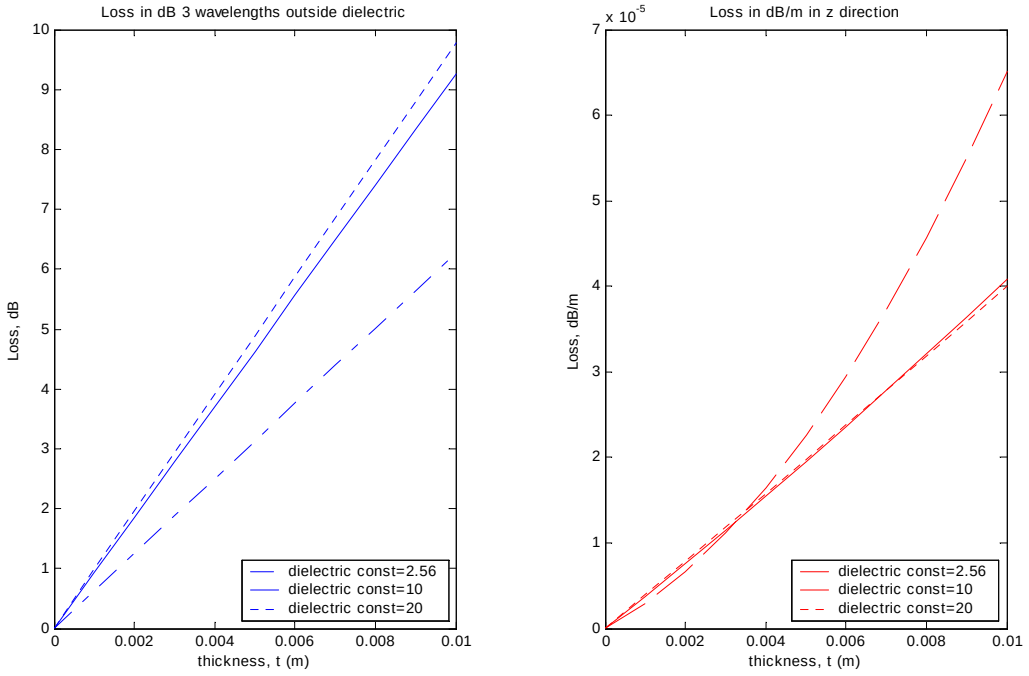

Figure 44. Decay at 3 λ_o and loss per meter for grounded dielectric slab with different dielectric constants and varying thickness.

The plot of the propagation loss in the *z* direction shows a linear increase in the propagation loss as the thickness of the dielectric coating increases. It also shows that for a given dielectric thickness, using a dielectric with constant 2.56 would yield a lower propagation loss compared to that for the higher dielectric constants. However, the magnitude of this propagation loss is in the order of 10^{-5} dB/m, which is much smaller than the 10^{-3} dB/m propagation loss for the parallel-plate. Although the results of the single conducting plane shows lower propagation loss compared to the parallel-plate waveguide, the simulation has not taken into account the possible coupling effects of the fields with nearby objects. The free space external coupling would cause interference to the wave propagation for the single conducting plane waveguide.

D. SUMMARY

This chapter discussed possible transmission systems for the array. The parallel-plate waveguide with the sandwiched dielectric medium and the single-plate conducting plane with a thin dielectric film were investigated. For the parallel-plate waveguide with a dielectric constant 2.0, the propagation loss was found to be negligible (in the range of 10^{-3} dB/m). As for the single conducting plane with a thin dielectric film, calculations show that the propagation loss is similar to the parallel plates. The research also showed that a two-dimensional cylindrical propagation would result in lower propagation loss over a three-dimensional spherical propagation.

VII. CONCLUSION AND RECOMMENDATIONS

A. CONCLUSIONS

Opportunistic phased array and aperstructures offer exciting new possibilities for military applications, especially surface warships. The design of these systems is expectedly complex. Low cost, high performance COTS systems should be leveraged to the fullest in the building of these systems.

As part of the task to demonstrate some crucial technologies in the laboratory using hardware at 2.4 GHz, the phase characteristics of the AD8347EVAL demodulator board were investigated. The suitability of the board as a demodulator on the receive end of an array T/R module was reiterated when used in complement with the AD8346EVAL modulator board on the transmit end. The digitization of the demodulator was also successfully implemented using the commercially available NI5112 digitizers. The research also successfully demonstrated a wireless LO distribution for a two-element transmit array. This is the first step towards a fully wireless opportunistic phased array. The transmission system for the sending and receiving of signals and control data between the beamformer and transmit/receive elements of the opportunistic array was also investigated. Investigations into the possible transmission systems for the aperstructure indicated that a two-dimensional cylindrical wave structure would incur significantly less propagation loss relative to three-dimensional spherical wave propagation. Parallel plate and grounded dielectric slab transmission systems were investigated. Both had very low loss per meter. However, the field outside of the dielectric layer can couple with external objects. A completely enclosed transmission structure like the parallel plates is more immune to interference and generates less electromagnetic interference (EMI) itself.

B. RECOMMENDATIONS FOR FUTURE WORK

1. Operational Amplifier in the Receive Module

To further improve the resolution of the phase samples from the demodulator, an operational amplifier can be used to boost the *I* and *Q* signal outputs. This will lessen the gain requirement for proper operation of the digitizers.

2. Receive Antenna Hardware

Upon the successful integration of the demodulator board, operational amplifier and the digitizer, the receive antenna can be constructed. This can be achieved by increasing the number of receive elements and integrating the outputs into the signal processor.

3. Signal Processing

The digital signal processing for the receive antenna can be investigated for the forming of the receive beams. With the completion of the receive antenna, the entire beam forming process from transmission to reception can then be verified.

4. Transmission System

Further research would be required into the transmission system for the aperstructure, with the determination of the field decay outside of the single conducting plane, and the effects of external coupling to the propagation loss.

APPENDIX. MATLAB CODES

This appendix contains all the MATLAB codes used in the research.

A. SIMULATION OF ARRAY FACTOR FOR N ELEMENT LINEAR ARRAY

```
% This MATLAB code calculates the array factor for N element linear array

clear all
close all

j=sqrt(-1);
c=3e08; % speed of light
fc=2.4e9; % carrier frequency
lamda1= c/fc; % wavelength
d=0.5*lamda1; % element spacing = half wavelength
k1=2*pi/lamda1; % propagation constant for signal at original frequency

N=50; % number of elements
theta0 = 30; %inital steer angle in degrees, measured from the array axis
increment=pi/10000; % increment of scan angle
theta=-pi/2:increment:pi/2; % scan from -pi/2 to pi/2
theta0= deg2rad(theta0); % to convert from degrees to radians

sum1=0;
for n=0:N-1
value1 = exp(j*(n*k1*d*(sin(theta)-sin(theta0))));
sum1 = sum1 + value1;
end

AF1=sum1/max(sum1); %normalised AF

figure(1)
plot(rad2deg(theta),20*log10(AF1),'k');
axis([-90 90 -50 0])
grid
ylabel('Relative power (dB)')
xlabel('\theta (degrees)')
```

B. PHASE RESPONSE OF AD8347EVAL DEMODULATOR

% This Matlab code is used to plot the graph to show the phase response of AD8347EVAL with and without VGIN set at 0.7V

```
clear
close all
sgn = 1;
ss = csvread('Measured 8347 17 Oct05 AGC 0.7V Demodulator board.csv'); sgn =1;

IP = ss(:,2);
IN = ss(:,3);
QP = ss(:,4);
QN = ss(:,5);

I = IP-IN;
Q = QP-QN;
I1 = I-mean(I);
Q1 = Q-mean(Q);

I1 = I1;%/max(I1);
Q1 = Q1;%/max(Q1);
ang = sgn*rad2deg(unwrap(atan2(Q1,I1)));

xaxis = 120:10:470;      % Sinsoidal plots for transmit phases are scaled and translated for comparison with results
A =0.4*(max(I)*(cos(xaxis*pi/180)))-0.045;
B =-0.36*(max(Q)*(sin(xaxis*pi/180)))+0.0225;

figure(1);
xaxis = 0:10:350;
%subplot(211); plot(xaxis,I1,xaxis,Q1)
subplot(211); plot(xaxis,IP,xaxis,IN);
title('IP,IN'), xlabel('Programmed phase (deg)');
ylabel('Voltage')
subplot(212); plot(xaxis,QP,xaxis,QN)
%title('QP,QN'), xlabel('Programmed Angle (deg)');
ylabel('Voltage')
figure(2);
xaxis = 0:10:350;
plot(xaxis,ang-min(ang),xaxis,xaxis,'+')
max(ang)-min(ang)
%title('Programmed Angle(degrees) vs Demodulated Angle(degrees)');
xlabel('Transmitted phase (degrees)'); ylabel('Received phase (degrees)')
legend('Received phase','Transmitted phase',2)
grid
figure(3);
xaxis = 0:10:350;
plot(xaxis,ang-min(ang)-xaxis.');
rms = std(ang-min(ang)-xaxis.')
%title(['Rms error between demodulated angle and programmed angle = ' num2str(rms) 'deg'])
xlabel('Transmitted phase (degrees)'); ylabel('Phase error (degrees)')
grid
figure(4);
xaxis = 0:10:350;
```

```
subplot(211);
plot(xaxis, I, xaxis, A, '+');    %
xlabel('Transmitted phase (degrees)'); ylabel('Measured differential In-Phase (volts)')
legend('Measured in-phase','Transmitted (Sinusoidal)',0)
subplot(212);
plot(xaxis, Q, xaxis, B, '*');
xlabel('Transmitted phase (degrees)'); ylabel('Measured differential Quadrature (volts)')
legend('Measured quadrature','Transmitted (Sinusoidal)',0)
```

C. MODELING OF MULTIPATHS

```
% This MATLAB code calculates the effects of multipaths inside a box
% Reflected path lengths between Source S and Observation points P in rectangular box
% Differential phase change at one of the observation points and Sum of E field from
% both observation points

clear
close all
rad=pi/180;

% box dimensions
xmin=0; xmax=50;
ymin=0; ymax=100;

% location of source (LO) in box
xs=25; ys=17;

% location of observation points in box
xp=[11.5 37.5]; yp=[50 50];
No=length(xp);      % No. of elements

% reflection coefficient of box walls
gam=[1 1 1 1]*0.316;    % 10dB = 10e(-10/20) abs

% location of images
X=[xs xmax+(xmax-xs) xs xmin-(xs-xmin)];
Y=[ymin-(ys-ymin) ys ymax+(ymax-ys) ys];

% reflected path lengths for all observation points
for n=1:No
   for i=1:4
      R(n,i)=sqrt((xp(n)-X(i))^2+(yp(n)-Y(i))^2);
   end
end

% Radar parameters
f=2.4e9;    % Hz
wavelength=3e8/f;
k=2*pi/wavelength;

% phase loop
p1=0; p2=360; dp=5;     % in deg
it=floor((p2-p1)/dp)+1;
for ii=1:it
```

```
   p=p1+(ii-1)*dp;
   P(ii)=(ii-1)*5;
   Phi(ii)=P(ii)*rad;  % in rad

% total reflected field at each observation point
for n=1:No
   summ=0;
   for i=1:4
   summ=summ+exp(-j*k*R(n,i))/R(n,i)*gam(i);
   end

% direct field at each observation point
Rd=sqrt((xp(n)-xs)^2+(yp(n)-ys)^2);
Ed(n,ii)=exp(-j*k*Rd)/Rd;

% sum of direct and reflected field at each observation point
E(n,ii)=summ+Ed(n,ii);
end
end

% Total E-field from both observation points (with amplitude imbalance)
Etot=E(1,:)+0.8*E(2,:).*exp(-j*Phi);     % 0.8 amplitude imbalance
Etotdb=20*log10(abs(Etot));

% plots
figure(1)   % Antenna setup in box
xb=[xmin xmax xmax xmin xmin];
yb=[ymin ymin ymax ymax ymin];
plot(xb,yb,xs,ys,'d',xp,yp,'o')
title('Box dimensions')
mx=max([max(xb) max(yb)]);
mn=min([min(xb) min(yb)]);
axis([mn mx mn mx]); axis square
legend('Wall', 'Source(LO)', 'Observation Points(Modulator Antennas)')
xlabel('x'), ylabel('y')

figure(2)   % Sum of E-field - Measured and Expected results
ss = csvread('Wireless LO.csv');
phase=ss(:,1);
power=ss(:,2);

for n=1:No
plot(P+3,Etotdb+25,'k-', phase, power, 'r:')    % Expected plot is translated for comparison
xlabel('Synchronization Phase, deg')
ylabel('Array Output, dB')
title('Array Output with Wireless LO distribution')
axis([p1 p2 -20 0])
legend('Expected', 'Measured',0)
hold on
end
hold off
```

D. AMPLITUDE VARIATION BETWEEN MODULATORS IN WIRELESS LO

```
% This MATLAB code simulates the effects of amplitude variation between modulators for
% the wireless LO
clear
close all
rad=pi/180;

% radar parameters
f=2.4e9;    % Hz
wavelength=3e8/f;
k=2*pi/wavelength;

% box dimensions
xmin=0; xmax=50;
ymin=0; ymax=100;

% location of source (LO) in box
xs=25; ys=17;

% location of observation points in box
xp=[11.5 37.5]; yp=[50 50];
No=length(xp);      % No. of elements

% reflection coefficient of box walls
gam=[1 1 1 1]*0.316;    % 10dB = 10e(-10/20) abs

% location of images
X=[xs xmax+(xmax-xs) xs xmin-(xs-xmin)];
Y=[ymin-(ys-ymin) ys ymax+(ymax-ys) ys];

% reflected path lengths for all observation points
for n=1:No
   for i=1:4
      R(n,i)=sqrt((xp(n)-X(i))^2+(yp(n)-Y(i))^2);
   end
end

%Phi=0;     % Fixed phase
Phi=pi/2;

% Amplitude loop; From 0 to 5V in 0.25V increment
a1=0; a2=5; da=0.25;
ia=floor((a2-a1)/da)+1;
for ii=1:ia
   a=a1+(ii-1)*da;
   A(ii)=(ii-1)*da;

% total reflected field at each observation point
for n=1:No
   summ=0;
   for i=1:4
   summ=(summ+exp(-j*k*R(n,i))/R(n,i)*gam(i));
   end
```

```
% direct field at each observation point
Rd=sqrt((xp(n)-xs)^2+(yp(n)-ys)^2);
Ed(n,ii)=exp(-j*k*Rd)/Rd;

% sum of direct and reflected field at each observation point
E(n,ii)=summ+Ed(n,ii);
end
end

% Total E-field from both observation points (with amplitude imbalance)
Etot=(5*E(1,:))+((A.*E(2,:)).*exp(-j*Phi));     % 0.8 amplitude imbalance
Etotdb=20*log10(abs(Etot));

figure(1)
% Measured results
%ss=csvread('Ampl_0.csv');
ss=csvread('Ampl_90.csv');
ampl_r=ss(1,:);
power_r=ss(2,:);

% Expected plot is scaled for comparison
for n=1:No
   plot(A,0.6*Etotdb+4.8,'b', ampl_r, power_r, 'r*')
   xlabel('Amplitude difference between receivers, V')
   ylabel('Array Output, dB')
   legend('Expected', 'Measured',0)
   axis([a1 a2 -20 0])
   hold on
end
hold off
```

E. TRANSMISSION LOSS IN PARALLEL PLATE TRANSMISSION

```
% This MATLAB code calculates the loss coefficient for parallel plate transmission
close
clear all

Freq=0.1e9:0.01e9:0.8e9;

Omega = 2*pi.*Freq;
mu = 1;
Parallel_Plate_Width_10 = 0.010;   % 10mm width
Parallel_Plate_Width_20 = 0.020;   % 20mm width
Parallel_Plate_Width_30 = 0.030;   % 30mm width
Permittivity_of_free_space = 8.854e-12;
Permeability_of_free_space = 12.6e-7;
Copper_Conductance = 5.8e7;
Dielectric_Constant=2.0;
Loss_Tangent=0.004;

Sigma=Loss_Tangent*Dielectric_Constant*Permittivity_of_free_space.*Omega;
Alpha_D=(Sigma./2).*sqrt(mu/Dielectric_Constant);
```

```
Alpha_C_10=(1/Parallel_Plate_Width_10).*((Permittivity_of_free_space*pi*Freq)./Copper_Conducta
nce).^0.5;
Alpha_C_20=(1/Parallel_Plate_Width_20).*((Permittivity_of_free_space*pi*Freq)./Copper_Conducta
nce).^0.5;
Alpha_C_30=(1/Parallel_Plate_Width_30).*((Permittivity_of_free_space*pi*Freq)./Copper_Conducta
nce).^0.5;

Loss_coefficient_10=exp(-(Alpha_C_10+Alpha_D));
Loss_coefficient_20=exp(-(Alpha_C_20+Alpha_D));
Loss_coefficient_30=exp(-(Alpha_C_30+Alpha_D));

dB_loss_per_unit_length_10=abs(20*log10(Loss_coefficient_10));
dB_loss_per_unit_length_20=abs(20*log10(Loss_coefficient_20));
dB_loss_per_unit_length_30=abs(20*log10(Loss_coefficient_30));

plot(Freq,dB_loss_per_unit_length_10,'k-')
hold
plot(Freq,dB_loss_per_unit_length_20,'b-.')
plot(Freq,dB_loss_per_unit_length_30,'r--')
grid
xlabel('Frequency, Hz')
ylabel('Loss coefficient, dB/m')
legend('Plate spacing, b=10mm','Plate spacing, b=20mm','Plate spacing, b=30mm',0)
% title('Transmission loss for dielectric between (copper) parallel plate')
```

F. 2D AND 3D TRANSMISSION LOSS

```
% This MATLAB code plots and compares the 2D and 3D transmission loss

clear
close all

l1=200;   % Max length (height) of boundary box (m)
l2=150;   % Max width of boundary box (m)

x=1:l2;
y=1:l1;

% Leg 1
x_1=0;
y_1=y;
R_1=sqrt(x_1.^2+y_1.^2);
rho_1=sqrt(x_1.^2+y_1.^2);
Power_1=10*log10(R_1.^2./rho_1);

% Leg 2
x_2=x;
y_2=l1;
R_2=sqrt(x_2.^2+y_2^2);
rho_2=l1+x_2;
Power_2=10*log10(R_2.^2./rho_2);

% Leg 3
x_3=l2;
```

```
y_3=l1:-1:1;
R_3=sqrt(x_3.^2+y_3.^2);
rho_3=l1+l2+(l1-y_3);
Power_3=10*log10(R_3.^2./rho_3);

subplot(131), plot(rho_1,Power_1); axis([0,200,0,25]);
xlabel('rho, m')
ylabel('Power, dB')
title('Leg 1')
hold
subplot(132), plot(rho_2,Power_2); axis([200,350,0,25]);
xlabel('rho, m')
ylabel('Power, dB')
title('Leg 2')
subplot(133), plot(rho_3,Power_3); axis([350,500,0,25]);
xlabel('rho, m')
ylabel('Power, dB')
title('Leg 3')
```

G. SINGLE CONDUCTING PLANE WITH THIN DIELECTRIC FILM

```
% This MATLAB is for the single conducting plane with thin dielectric film
% It plots propagation loss and attenuation at 3-wavelength from surface
clear
close all
format short
rad=pi/180;
sig=5.8e7;  % conductivity
f=3e8;      % frequency
c=3e8;
w0=c/f;     % (m) wavelength
k0=2*pi/w0;
Z0=377;

% polystyrene dielectric layer
erp=2.56;
erp_10=10;
erp_20=20;
erpp=.002;
er=erp-j*erpp;
er_10=erp_10-j*erpp;
er_20=erp_20-j*erpp;
t=0:0.001:.01;     % (m) thickness

% surface impedance of conductor (normalised)
Rs=sqrt(k0/2/sig/Z0);
Xs=Rs;
Zs=Rs+j*Xs;

% traverse wave no. in free space
h1=k0*(Zs+j*k0*t*(er-1)/er);
h1_10=k0*(Zs+j*k0*t*(er_10-1)/er_10);
h1_20=k0*(Zs+j*k0*t*(er_20-1)/er_20);
h1p=real(h1); h1pp=imag(h1);
```

```
h1p_10=real(h1_10); h1pp_10=imag(h1_10);
h1p_20=real(h1_20); h1pp_20=imag(h1_20);

% loss at 3-wavelength distance
Lxdb=-20*log10(exp(-h1pp*3*w0));
Lxdb_10=-20*log10(exp(-h1pp_10*3*w0));
Lxdb_20=-20*log10(exp(-h1pp_20*3*w0));

figure(1)
subplot(121); plot(t,Lxdb,'b-.',t,Lxdb_10,'b',t,Lxdb_20,'b:')
xlabel('thickness, t (m)')
ylabel('Loss, dB')
legend('dielectric const=2.56','dielectric const=10','dielectric const=20',4)
title('Loss in dB 3 wavelengths outside dielectric')
hold

% loss per meter in the z direction
beta=sqrt(k0.^2-h1.^2);   % propagation factor
beta_10=sqrt(k0.^2-h1_10.^2);
beta_20=sqrt(k0.^2-h1_20.^2);
bp=real(beta); bpp=imag(beta);
bp_10=real(beta_10); bpp_10=imag(beta_10);
bp_20=real(beta_20); bpp_20=imag(beta_20);
Lzdb=-20*log10(exp(bpp*1));
Lzdb_10=-20*log10(exp(bpp_10*1));
Lzdb_20=-20*log10(exp(bpp_20*1));

subplot(122); plot(t,Lzdb,'r-.',t,Lzdb_10,'r',t,Lzdb_20,'r:')
xlabel('thickness, t (m)')
ylabel('Loss, dB/m')
legend('dielectric const=2.56','dielectric const=10','dielectric const=20',4)
title('Loss in dB/m in z direction')
```

THIS PAGE INTENTIONALLY LEFT BLANK

LIST OF REFERENCES

[1] US Navy - Future Surface Combatant Program, http://peoships.crane.navy.mil/ddx/default.htm, November 2005.

[2] L. C. Esswein, "Genetic algorithm design and testing of a random element 3-D 2.4 GHz phased array transmit antenna constructed of commercial RF microchips," Master's Thesis, Naval Postgraduate School, Monterey, California, June 2003.

[3] Cher Sing, Eng, "Digital antenna architectures using commercial off the shelf hardware," Master's Thesis, Naval Postgraduate School, Monterey, California, December 2003.

[4] Chin Siang, Ong, "Digital phased array architectures for radar and communications based on off-the-shelf wireless technologies," Master's Thesis, Naval Postgraduate School, Monterey, California, December 2004.

[5] W. L. Stutzman and G. A. Thiele, *Antenna Theory and Design*, 2nd Edition, Wiley, New York, 1998.

[6] R. C. Hansen, *Phased Array Antennas*, Wiley, New York, 1998.

[7] C. A. Balanis, *Antenna Theory Analysis and Design*, 2nd edition, Wiley, New York, 1997.

[8] N. Fourikis, *Advanced Array Systems, Applications and RF Technologies*, Associated Press, San Diego, 2000.

[9] M. I. Skolnik, *Introduction to Radar Systems*, 3rd edition, McGraw-Hill, New York, 2001.

[10] C. H. Tong, "System study and design of broad-band U-slot microstrip patch antennas for aperstuctures and opportunistic arrays," Master's Thesis, Naval Postgraduate School, Monterey, California, December 2005.

[11] D. C. Jenn, Presentation notes: *Aperstructures, Opportunistic Arrays and BMD*, Naval Postgraduate School, October 2005 (unpublished).

[12] Analog Devices AD8347 Quadrature Demodulator, http://www.analog.com/UploadedFiles/Data_Sheets/230407246AD8347_a.pdf, October 2005.

[13] Analog Devices AD8346 Quadrature Modulator, http://www.analog.com/UploadedFiles/Data_Sheets/240325465AD8346_a.pdf, October 2005.

[14] J. Maloney and J. Schultz, Presentation notes: *Aperstructures – Advance Integrated Antennas for Ship Topsides*, Georgia Tech Research Institute, September 2004 (unpublished).

[15] D. K. Cheng, *Field and Wave Electromagnetics*, 2nd edition, Addison-Wesley, Massachusetts, 1992.

[16] R. E. Collin, *Field Theory of Guided Waves*, 2nd edition, IEEE Press, New York, 1991.

INITIAL DISTRIBUTION LIST

1. Defense Technical Information Center
   Ft. Belvoir, Virginia

2. Dudley Knox Library
   Naval Postgraduate School
   Monterey, California

3. Professor David C. Jenn
   Department of Electrical & Computer Engineering
   Naval Postgraduate School
   Monterey, California

4. Professor Donald L. Walters
   Physics Department
   Naval Postgraduate School
   Monterey, California

5. Professor Andres Larraza
   Physics Department
   Naval Postgraduate School
   Monterey, California

6. Chairman, Physics Department
   Naval Postgraduate School
   Monterey, California

7. James King
   Office of Naval Research
   Arlington, Virginia

8. Professor Michael Melich
   Wayne E. Meyer Institute of System Engineering
   Naval Postgraduate School
   Monterey, California

9. Professor Rodney Johnson
   Wayne E. Meyer Institute of System Engineering
   Naval Postgraduate School
   Monterey, California

10. Yeo Siew Yam
    DSO National Labs
    Singapore

11. Professor Yeo Tat Soon
Director of Temasek Defence System Institute
National University of Singapore
Singapore

12. Leo Tin Boon
Temasek Defence System Institute
National University of Singapore
Singapore

13. LCDR Gert Burgstaller
Code: EC596
Naval Postgraduate School
Monterey, California

14. MAJ Loke Yong
Naval Postgraduate School
Monterey, California

15. LTC Yong, Yoke Chuang
Ministry of Defence
Singapore